








YSL3-mediated copper distribution is required for fertility, seed size and protein accumulation in *Brachypodium*

Huajin Sheng,^{1,2} Yulin Jiang,^{1,2} Maryam Rahmati,¹ Ju-Chen Chia ,¹ Tatyana Dokuchayeva ,³ Yana Kavulych ,^{1,4} Tetiana-Olena Zavodna,¹ Patrick N. Mendoza ,^{1,5} Rong Huang ,⁶ Louisa M. Smieshka,⁶ Julia Miller,^{5,7} Arthur R. Woll,⁶ Olga I. Terek,⁴ Nataliya D. Romanyuk ,⁴ Miguel Piñeros,^{5,7} Yonghong Zhou^{2,†} and Olena K. Vatamaniuk ,^{1,5,*†}

- 1 Soil and Crop Sciences Section, School of Integrative Plant Science, Cornell University, Ithaca, NY 14853, USA
- 2 Triticeae Research Institute, Sichuan Agricultural University, Wenjiang, Sichuan 611130, China
- 3 Cornell Nutrient Analysis Laboratory, School of Integrative Plant Science, Cornell University, Ithaca, NY 14853, USA
- 4 Department of Biology, Ivan Franko National University of Lviv, Lviv 79005, Ukraine
- 5 Plant Biology Section, School of Integrative Plant Science, Cornell University, Ithaca, NY 14853, USA
- 6 Cornell University, Cornell High Energy Synchrotron Source (CHESS), Ithaca, NY 14853, USA
- 7 Robert W. Holley Center for Agriculture and Health, USDA-ARS, Ithaca, NY 14853, USA

*Author for communication: okv2@cornell.edu

†Senior authors.

O.K.V. designed experiments with H.S.; H.S., Y.J., M.R.I., J.-C.C., P.M., T.Z., and Y.K., performed experiments; T.D. assisted in ICP-MS analysis; J.M. and M.P. performed studies in oocytes; R.H., L.S., and A.W. facilitated the SXRF experiments at CHESS and NSLSII (Brookhaven National labs). Y.Z., O.I.T., N.D.R. contributed to discussion on the manuscript. The manuscript was written by O.K.V., H.S. with contribution from M.P. All authors contributed constructive comments on the manuscript.

The author responsible for distribution of materials integral to the findings presented in this article in accordance with the policy described in the Instructions for Authors (<https://academic.oup.com/plphys/pages/general-instructions>) is: Olena K. Vatamaniuk (okv2@cornell.edu).

Abstract

Addressing the looming global food security crisis requires the development of high-yielding crops. In agricultural soils, deficiency in the micronutrient copper significantly decreases grain yield in wheat (*Triticum aestivum*), a globally important crop. In cereals, grain yield is determined by inflorescence architecture, flower fertility, grain size, and weight. Whether copper is involved in these processes, and how it is delivered to the reproductive organs is not well understood. We show that copper deficiency alters not only the grain set but also flower development in both wheat and its recognized model, *Brachypodium distachyon*. We then show that the *Brachypodium* yellow stripe-like 3 (YSL3) transporter localizes to the phloem, transports copper in frog (*Xenopus laevis*) oocytes, and facilitates copper delivery to reproductive organs and grains. Failure to deliver copper, but not iron, zinc, or manganese to these structures in the *ysl3* CRISPR-Cas9 mutant results in delayed flowering, altered inflorescence architecture, reduced floret fertility, grain size, weight, and protein accumulation. These defects are rescued by copper supplementation and are complemented by YSL3 cDNA. This knowledge will help to devise sustainable approaches for improving grain yield in regions where soil quality is a major obstacle for crop production. Copper distribution by a phloem-localized transporter is essential for the transition to flowering, inflorescence architecture, floret fertility, size, weight, and protein accumulation in seeds.

Introduction

Global food security and the demand for high-yielding grain crops are among the most urgent drivers of modern plant sciences due to the current trend of population growth, extreme weather conditions, and decreasing arable land resources (Godfray et al., 2010). The grain yield is directly linked to the crop and soil fertility. In this regard, it has been known for decades that the deficiency for the micronutrient copper in alkaline, coarse-textured, or organic soils that occupy more than 30% of the world arable land, compromises crop fertility, reduces grain/seed yield, and in acute cases results in crop failure (Graham, 1978; Shorrocks and Alloway, 1988; Solberg et al., 1999; White and Broadley, 2009; Broadley et al., 2012; Mitra, 2015). In accord with the essential role of copper in reproduction, recent studies using synchrotron X-ray fluorescent (SXRF) microscopy established that copper localizes to anthers and pistils of flowers in a model dicotyledonous species, *Arabidopsis thaliana*, and failure to deliver copper to these reproductive organs severely compromises fertility and seed set (Yan et al., 2017; Rahmati Ishka and Vatamaniuk, 2020). Although copper deficiency can be remedied by the application of copper-based fertilizers, this approach is not environmentally friendly and can lead to the buildup of toxic copper levels in soils (Shorrocks and Alloway, 1988; Solberg et al., 1999; Burkhead et al., 2009). Mineral nutrient transporters have been recognized as key targets for improving the mineral use efficiency in sustainable crop production (Schroeder et al., 2013). Wheat (*Triticum aestivum*) is the world's third important staple crop after maize (*Zea mays*) and rice (*Oryza sativa*); however, wheat grain yield remained relatively low under marginal growing environments despite significant breeding efforts (Tshikunde et al., 2019). Wheat is also regarded as the most sensitive to copper deficiency (Graham, 1978; Shorrocks and Alloway, 1988; Solberg et al., 1999; Mitra, 2015). How copper uptake and internal transport is achieved in wheat and how it affects fertility is poorly understood. Based on studies in *A. thaliana*, copper uptake and internal distribution are mediated by members of the **Copper Transporter (COPT)** family, **Heavy Metal Transporting P_{1B}-type ATPases (HMAs)**, and members from the **Yellow Stripe-like (YSL)** subfamily of the **Oligopeptide Transporter (OPT)** family (Kampfenkel et al., 1995; Sancenon et al., 2003; DiDonato et al., 2004; Abdel-Ghany et al., 2005; Waters et al., 2006; Burkhead et al., 2009; Chu et al., 2010; Jung et al., 2012; Gayomba et al., 2013). Most of these transporters are transcriptionally upregulated by copper deficiency by a conserved transcription factor, SPL7 (Squamosa Promoter-Binding Protein-like7), and a newly identified transcription factor CTF1 (Copper Deficiency-induced Transcription Factor1; Yamasaki et al., 2009; Bernal et al., 2012; Yan et al., 2017). The expression of several COPT family members is also induced in roots by copper deficiency in *O. sativa* and an emerging wheat model *Brachypodium distachyon* (from here on, brachypodium), and several brachypodium COPTs mediate low-affinity

copper uptake (Yuan et al., 2011; Jung et al., 2014). A member of the YSL transporters, OsYSL16 functions in the phloem-based copper delivery to reproductive organs in rice (Schwacke et al., 2003; Zheng et al., 2012; Zhang et al., 2018). Other studies, however, reported that OsYSL16 functions mainly in the distribution of iron (Kakei et al., 2012; Lee et al., 2012). Recognizing the limitations of wheat for functional genetics studies due to polyploidy, lower transformation rates, and longer life cycle, we used brachypodium as a wheat proxy (Yordem et al., 2011; Jung et al., 2014; Scholthof et al., 2018) for the study of copper transport processes and their role in establishing yield traits. We show that copper deficiency alters not only the grain set but also flower development in both wheat and brachypodium. Of 19 YSL family members in brachypodium, we focused on BdYSL3, which has the closest sequence similarity to OsYSL16, AtYSL1, and AtYSL3 (Yordem et al., 2011). We reveal that brachypodium yellow-stripe-like 3 (BdYSL3) protein localizes to the plasma membrane, transports copper ions in the heterologous systems, and mediates phloem-based copper delivery to flag leaves, anthers, and pistils of florets. Loss of this function in the *ysl3* mutant results in a delayed flowering, altered inflorescence architecture, reduced floret fertility, grain number, size, weight and protein accumulation. These defects are rescued by copper supplementation and are complemented by the *BdYSL3* cDNA. Our results suggest that the manipulation of *BdYSL3* and other-like proteins has the potential to play a role in devising sustainable and environmentally friendly approaches for improving wheat and other cereal grain yields and thus, food security.

Results

Copper deficiency significantly decreases flower formation and seed yield in wheat and *Brachypodium*

We first evaluated the growth and fertility of wheat and brachypodium grown under different concentrations of copper to validate using brachypodium as a wheat model in this study. Omitting copper from the hydroponic medium severely stunted the growth, tiller, head, flower, and seed/grain formation per plant in both wheat and brachypodium (Fig. 1 and Supplemental Fig. 1). Seeds were also not formed under low (10 nM) copper in both species (Fig. 1F, H); tillers, heads, and flowers were formed albeit at a reduced level (Fig. 1E, G and Supplemental Fig. 1C–F). Notably, seed formation was also significantly reduced (by 87%) in both wheat and brachypodium when plants were grown under 50 nM copper, although flower formation was only somewhat reduced compared to plants grown under copper replete conditions (125, 250 nM copper, Fig. 1E–H). These data show that copper deficiency impacts different aspects of reproductive development, including flower and seed/grain formation, with the most dramatic effect on seeds/grain production. Furthermore, these data supported the applicability of using brachypodium for the study of the relationship between copper and fertility in cereals, as well as

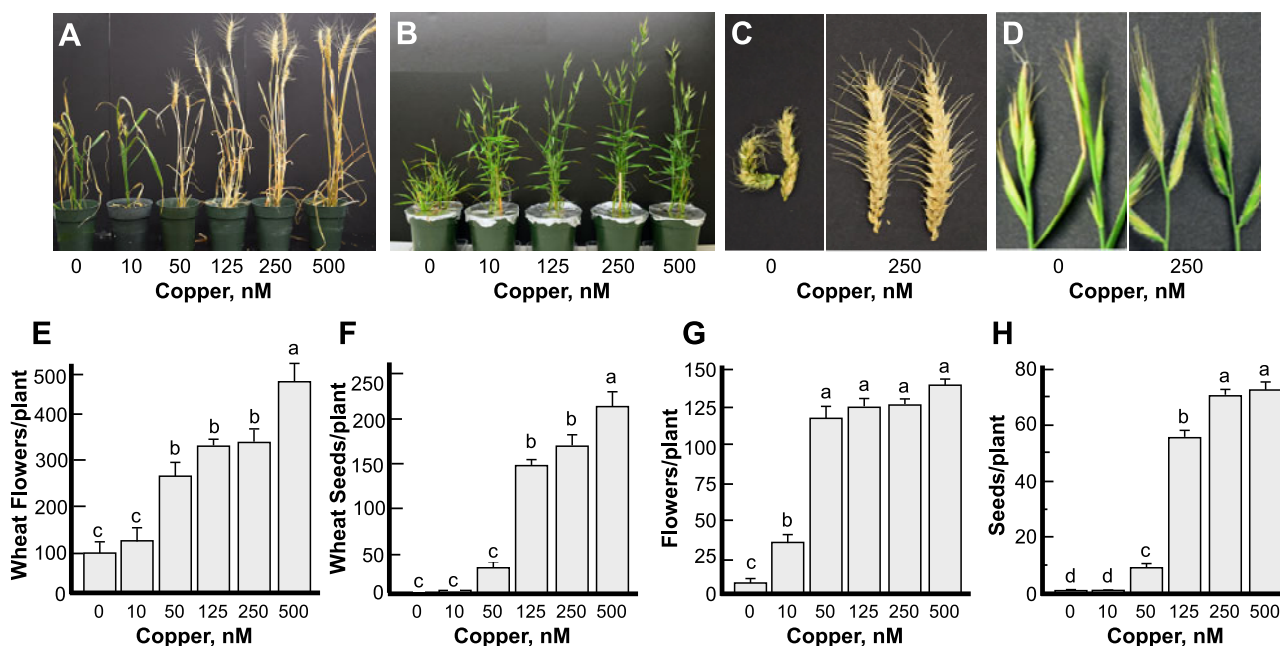


Figure 1 Copper deficiency alters flower development and reduces grain number in wheat and brachypodium. Plants were grown hydroponically under indicated copper concentrations. (A–D) Representative images of plants, tiller and head appearance under different copper concentrations of wheat (A, C) and brachypodium (B, D). (E–H) The number of flowers and grains per plant in wheat (E, F) or brachypodium (G, H). Statistical analysis in (E–H) was done with one-way ANOVA in the JMP Pro 14 software package; comparison of the means for all pairs was done using Tukey–Kramer HSD test. Data in (E–H) show mean values \pm S.E. from the analysis of four (wheat) to six (brachypodium) independently grown plants from one out of two (wheat) and three (brachypodium) independent experiments. Levels not connected by the same letter are significantly different ($p < 0.05$, Tukey–Kramer HSD test).

the identification of transport pathways responsible for the delivery of copper to plant reproductive organs.

Copper deficiency increases the transcript abundance of *BdYSL3*

We then focused on brachypodium YSL3 because its counterparts in *Arabidopsis* and rice contribute to the transport of transition metals, including copper (Waters et al., 2006; Yordem et al., 2011; Zheng et al., 2012; Zhang et al., 2018). We found that *BdYSL3* was expressed in different plant organs including roots, leaves, nodes, and reproductive organs (Fig. 2A). The highest expression of *BdYSL3* was observed in young leaves of four-week-old seedlings, followed by flag leaves at the flowering stage and mature leaves at jointing (Fig. 2A). *BdYSL3* was also expressed in different flower organs including lemma, palea, and ovaries, but the abundance of the transcript was much lower than in leaves (Fig. 2A).

We then found that *BdYSL3* was highly upregulated under copper deficiency in roots, stems, and mature leaves but not in young leaves of four-week-old plants. Copper deficiency also significantly increased the transcript abundance of *BdYSL3* in flag leaves and flowers at the reproductive stage (Fig. 2B). These results suggested that *BdYSL3* might be involved in internal copper distribution and delivery to reproductive organs when copper is limited.

Because of conflicting reports in the literature regarding the regulation and transport capabilities of *BdYSL3*

counterpart in rice, *OsYSL16* (Kakei et al., 2012; Lee et al., 2012; Zheng et al., 2012; Zhang et al., 2018), we tested the effect of iron deficiency on the expression of *BdYSL3*. We found that iron deficiency downregulated the transcript abundance of *BdYSL3* in both roots and leaves of brachypodium (Fig. 2C).

BdYSL3 is expressed mainly in the phloem and localizes to the plasma membrane

We next examined the tissue and cell-type specificity of *BdYSL3* expression using brachypodium transformed with the *BdYSL3_{pro}-GUS* construct. We found that *BdYSL3* is expressed predominantly in the vascular tissues of roots and leaves of plants subjected to copper deficiency (Fig. 3A, B). The bulk of GUS staining was associated with the phloem of large and small longitudinal veins as well as in mesophyll parenchyma cells (Fig. 3C). Because nodes of grasses are regarded as hubs directing metal distribution (Yamaji and Ma, 2014), we also evaluated *BdYSL3_{pro}-GUS* activity in the node I. GUS activity was observed mainly in large vascular bundles of the node (Fig. 3D). Within the large vascular bundles, where the xylem and the phloem are located on the inside and the outside, respectively, GUS staining was mainly associated with the phloem and also was found in parenchyma cells (Fig. 3E). Concerning florets, GUS activity was observed in the ovary, styles (Fig. 3F), the vasculature of the lemma (Fig. 3G), but not in anthers and palea. GUS activity was undetectable in any of the tissues of plants grown

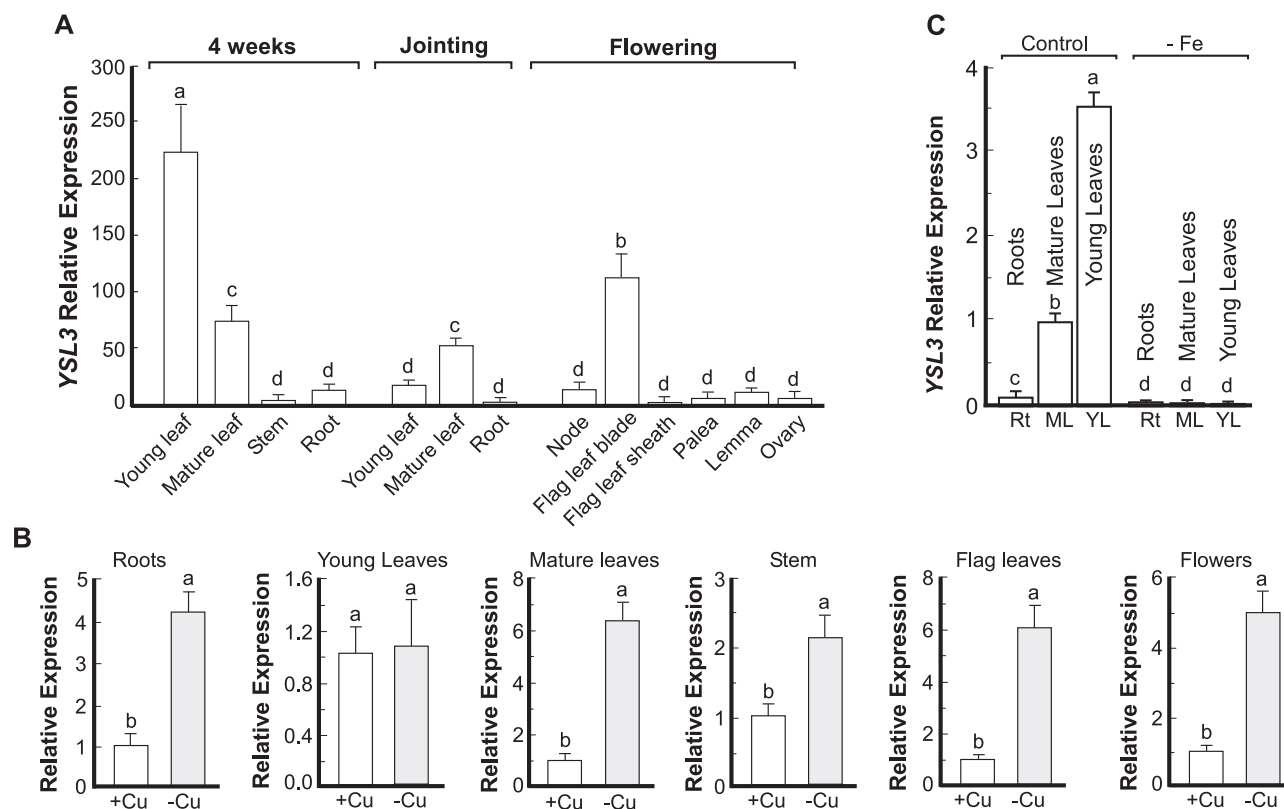


Figure 2 Copper deficiency increases transcript abundance of *BdYSL3*. **(A)** The expression level of *BdYSL3* in different tissues at different growth stages. Wild-type brachypodium was grown hydroponically under copper sufficient (0.25 μM CuSO_4) conditions. The indicated plant tissues were collected at the indicated time and developmental stage; RNA was extracted and subjected to RT-qPCR analysis. **(B)** The expression level of *BdYSL3* in different tissues of brachypodium wild-type grown hydroponically under copper sufficient (+Cu) or deficient conditions (-Cu) conditions. Young (two uppermost leaves) and mature leaves (the remaining leaves), stems, and roots were collected from four-week-old plants. Flag leaves and flowers were collected from six-week-old plants. In all cases, the copper deficiency was achieved by transferring plants to a fresh medium lacking copper one week before tissue sampling. **(C)** Plants were grown hydroponically for two weeks before transferring to a medium without iron. Tissues were collected from three-week-old plants for subsequent RNA extraction, cDNA synthesis, and RT-qPCR. **Rt**, roots; **ML**, mature leaves; **YL**, young leaves. Shown values are arithmetic means \pm S.E. ($n = 3$ independent experiments with tissues pooled from three plants per experiment. Levels not connected by same letter are significantly different ($p < 0.05$, Tukey-Kramer HSD test).

under copper sufficient conditions. The predominant expression of *BdYSL3* in the phloem, phloem parenchyma cells, and mesophyll suggested that *BdYSL3* is involved in internal copper distribution rather than copper uptake into the roots. We next found that *BdYSL3* localizes to the plasma membrane (PM; Fig. 4), suggesting that it is involved in the movement of substrates into or out of the cell rather than subcellular (e.g. vacuolar) sequestration.

BdYSL3 facilitates copper uptake in *Xenopus oocytes*

To test the transport capabilities of *BdYSL3*, we employed *Xenopus laevis* oocytes. We first examined the cellular localization of *BdYSL3* expressed in this heterologous system. Confocal microscopy of oocytes injected with the complementary RNA (cRNA) of the YFP::*BdYSL3* fusion protein revealed the YFP signal of the protein chimera at the cell periphery, co-localizing with the Deep Red PM marker (Fig. 5A). In contrast, water-injected cells showed no fluorescence background signal. Having validated that *BdYSL3* localizes to the PM in oocytes as it does in *A. thaliana* protoplasts

(Fig. 4), we performed the transport characterization of the untagged *BdYSL3* by analyzing copper uptake in *BdYSL3*-expressing oocytes. Given that members of the OPT family have been shown to transport transition metals as ions and a metal-nicotianamine (NA) or metal-phytosiderophores (PS) complexes (DiDonato et al., 2004; Schaaf et al., 2004; Zhai et al., 2014), we provided copper as Cu^{2+} (CuSO_4) or as Cu-NA (copper-NA). Differences in Cu^{2+} uptake between control and *BdYSL3*-expressing cells were detected after 1 hour of incubation of oocytes in the Cu^{2+} containing bathing solution, with the magnitude of *BdYSL3*-mediated Cu^{2+} uptake increasing in a time-dependent manner (Fig. 5B). In contrast, when copper was provided as Cu-NA complex, no significant copper uptake was detected in *BdYSL3*-expressing cells, relative to the background levels observed in control cells (Fig. 5C).

To further demonstrate that the prepared Cu-NA complexes supplied in the assay were available for transport, we have used the maize YS1 (*ZmYS1*) as a positive control because it was established previously that this transporter is

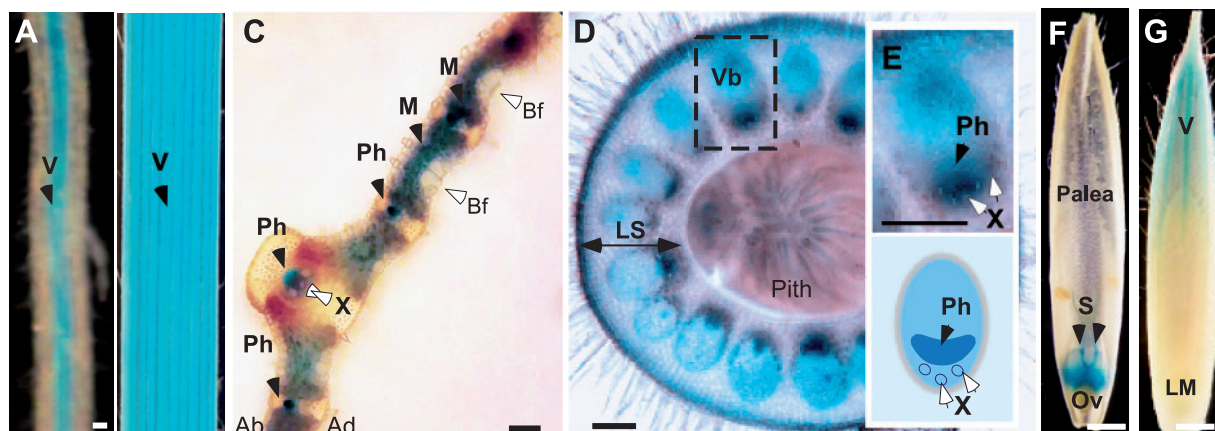


Figure 3 Tissue-specificity of the expression of *BdYSL3*. Transgenic plants expressing *BdYSL3_{pro}*-GUS construct were grown hydroponically for three (A–C) or six (D–G) weeks. Plants were transferred to hydroponic solution without copper (–Cu) for one week prior to histochemical analysis. (A, B) Representative images of GUS staining in the vasculature (V, black arrow) of lateral roots and the third emerged leaf, respectively. Transverse sections through a leaf lamina (C) and a node (D) show GUS staining in tissues indicated by black arrows. (E) Top image shows a close-up of a vascular bundle embedded in a dashed box in (D). Lower image shows the distribution of the phloem and the xylem in the vascular bundle. (F) GUS staining in dissected flowers of *BdYSL3_{pro}*-GUS-expressing transgenics grown under copper deficiency. (G) GUS staining in the vasculature of the lemma of plants grown under copper deficiency. X-xylem vessels; Ph, phloem; Vb, vascular bundle; LS, leaf sheath of the node; V, vasculature; S, styles of pistils; Ov, ovary; LM, lemma; Bf, bulliform cells; Ad, adaxial side of the leaf lamina; Ab, abaxial side of the leaf lamina. *BdYSL3_{pro}*-GUS-mediated staining is indicated by black arrows. Open arrows point to other tissues and cell types. GUS staining was not detected in plants grown under copper sufficient conditions. Scale bars: 100 μ m in A, C, D, E and 1 mm in B, F, G.

capable of transporting metal–NA complex in oocytes (Schaaf et al., 2004). Consistent with past findings (Schaaf et al., 2004), ZmYS1 was capable of transporting Cu–NA complex as evidenced by 1.8-fold higher copper accumulation in ZmYS1-expressing versus mock-treated cells (Fig. 5C). These data show that the inability of *BdYSL3* to transport Cu–NA is not associated with artifacts from the preparation of the Cu–NA complex. Intriguingly, we also found that similar to *BdYSL3*, ZmYS1 was capable of facilitating the uptake of copper, provided as CuSO_4 (Fig. 5C). Furthermore, ZmYS1-expressing cells accumulated 1.6-fold more copper when it was provided as CuSO_4 rather than Cu–NA. Together, our results show that *BdYSL3* is capable of transporting free Cu^{2+} in oocytes. In addition, we show that free Cu^{2+} ions but not the Cu–NA complex are the preferred transport substrates for *BdYSL3* and ZmYS1 at least in the *Xenopus* oocyte heterologous system.

The *ysl3-3* mutant of brachypodium is sensitive to copper deficiency

We then generated *ysl3* deletion mutants using the CRISPR/CAS9 (clustered regularly interspaced short palindromic repeats [CRISPR]) approach (Supplemental Information and Supplemental Figs. 2A and 3). After obtaining Cas9-free mutant lines (Supplemental Figure 2B, C), positions of deletion breakpoints were established by sequencing. Three alleles bearing 122, 123, and 182 bp deletions encompassing a part of the 5'UTR and the first exon of *BdYSL3* were identified and designated as *ysl3-1*, *ysl3-2*, and *ysl3-3*, respectively

(Supplemental Information online and Supplemental Figures 2A, E). Plants of all alleles were smaller than wild-type when they were grown under copper sufficient conditions (Supplemental Figure 2D). Given the essential role of copper in plant growth and development, and because *BdYSL3* is capable of transporting copper (Fig. 5), we hypothesized that *ysl3* mutant lines experience copper deficiency and thus are smaller than wild-type under copper replete conditions.

We then used the *ysl3-3* allele, for the in-depth studies and generated two *ysl3-3* transgenic lines expressing *BdYSL3* cDNA, *ysl3/YSL3-1*, and *ysl3/YSL3-2*, for functional complementation assays. The level of *BdYSL3* transcript was increased in both *ysl3/YSL3-1* and *ysl3/YSL3-2* lines compared to the wild-type (Supplemental Figure 4). We next compared the growth of the *ysl3-3* mutant versus wild-type and *ysl3/YSL3-1* and *ysl3/YSL3-2* plants in the medium with versus without copper. As evident by the smaller stature of the *ysl3-3* plants (Fig. 6A), curling of their leaf margins (Fig. 6B), and decreased height of shoots (Fig. 6C), the *ysl3-3* mutant was more sensitive to copper deficiency than the wild-type. The dry weight of shoots and roots of the *ysl3-3* mutant was significantly different from wild-type even when plants were grown under copper sufficiency and omitting copper from the medium did not change it further (Fig. 6D, E). Importantly, the expression of *BdYSL3* cDNA in the *ysl3-3* mutant rescued all defects of the mutant (Fig. 6A–E) suggesting that slower growth of the *ysl3-3* plants under control conditions and further reduced growth under copper deficiency were due to the loss of the *BdYSL3* gene. The *ysl3-3*

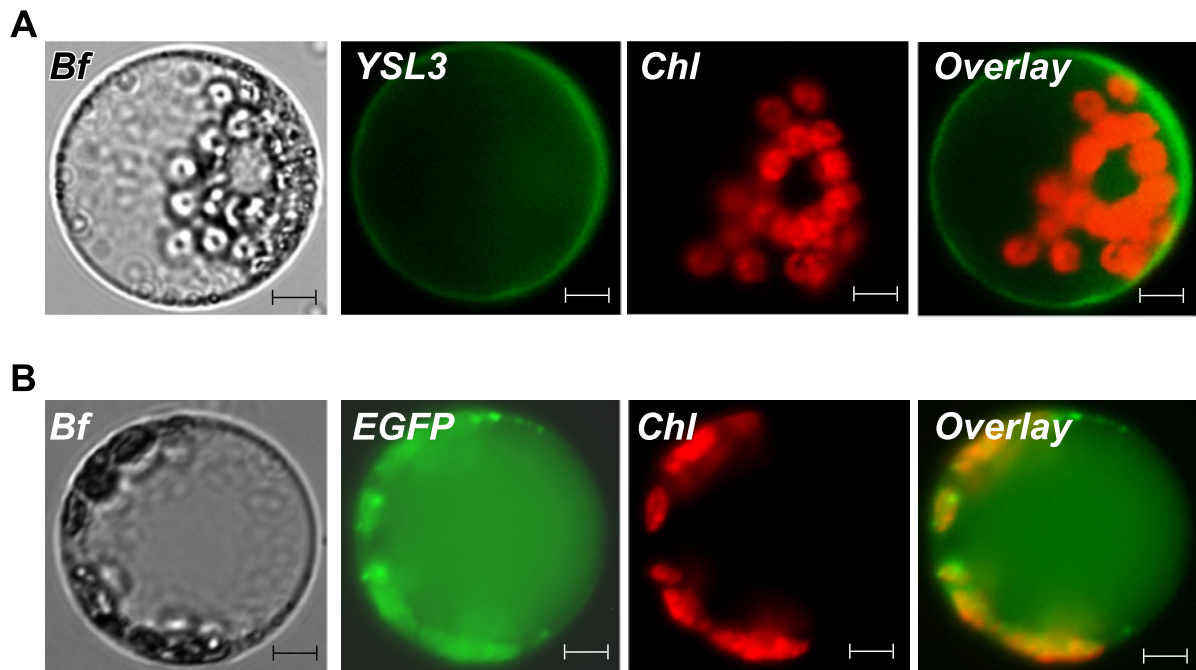


Figure 4 BdYSL3 localizes to the plasma membrane in *Arabidopsis thaliana* protoplast. BdYSL3 fused with EGFP at the C-termini (A) or EGFP-expressing empty vector (B) was transfected into protoplasts prepared from *A. thaliana* mesophyll cells. Shown are a bright-field image (Bf) of transfected protoplasts, BdYSL3-EGFP (YSL3)-mediated fluorescence, EGFP (EGFP)-mediated fluorescence and chlorophyll autofluorescence (Chl) fluorescence. Overlay images were created to show that BdYSL3-EGFP-mediated fluorescence does not co-localize with the chlorophyll-mediated fluorescence. Scale bar = 5 μm .

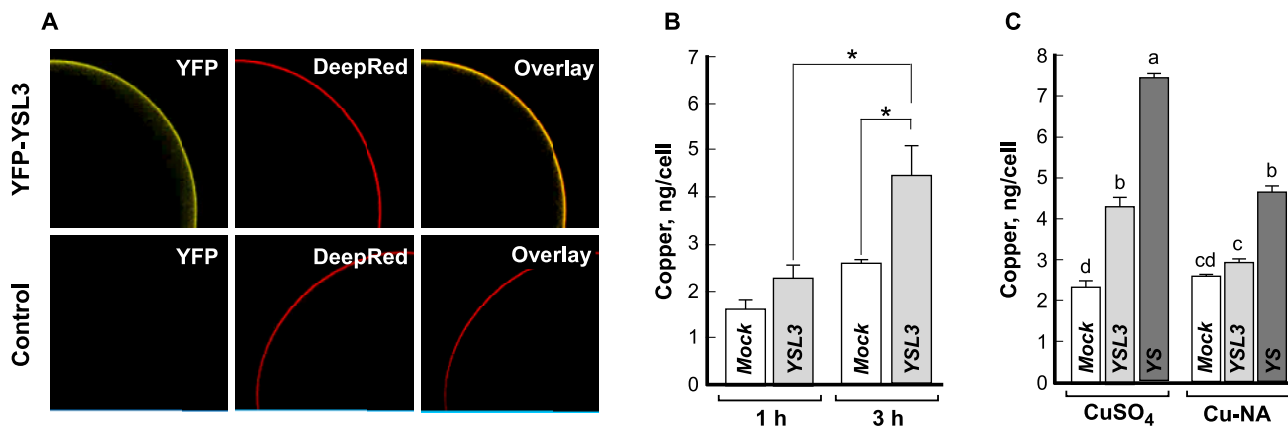


Figure 5 BdYSL3 mediates copper uptake in *Xenopus laevis* oocytes. (A) YFP::BdYSL3 localizes to the plasma membrane in *X. laevis* oocytes, as evidenced by its co-localization with the Deep Red plasma membrane marker (upper panel). Plasma membrane staining by Deep Red in control (i.e. water-injected) cells and the lack of YFP autofluorescence are shown for reference in the lower panel. (B, C) Copper uptake into oocytes injected with either *BdYSL3* cRNA (YSL3; B, C), *ZmYS* cRNA (YS; C), or water (Mock; B, C). Copper uptake was measured at 1 or 3 h (B) or 3 h (C). The basal uptake solution was supplemented with 100 μM CuSO_4 (B), 100 μM CuSO_4 or 100 μM Cu-NA (C). Presented values are arithmetic means \pm S.E. ($n = 5\text{--}6$). Asterisks in (B) indicate statistically significant differences (*, $p < 0.05$; **, $p < 0.01$, Student's *t* test); levels not connected by the same letters in (C) are statistically significant ($p < 0.05$, Tukey–Kramer HSD test).

mutant was not more sensitive to manganese, iron, or zinc deficiencies compared to wild-type (Supplemental Figure 5). Together, these results indicate that *BdYSL3* is essential for the normal growth of brachypodium under control condition and under copper deficiency.

The *ysl3-3* mutant has a delayed flowering time and produces more spikelets and florets per inflorescence

We then grew wild-type, the *ysl3-3* mutant and *ysl3/YSL3-1* and *ysl3/YSL3-2* plants in soil to evaluate the role of *BdYSL3*

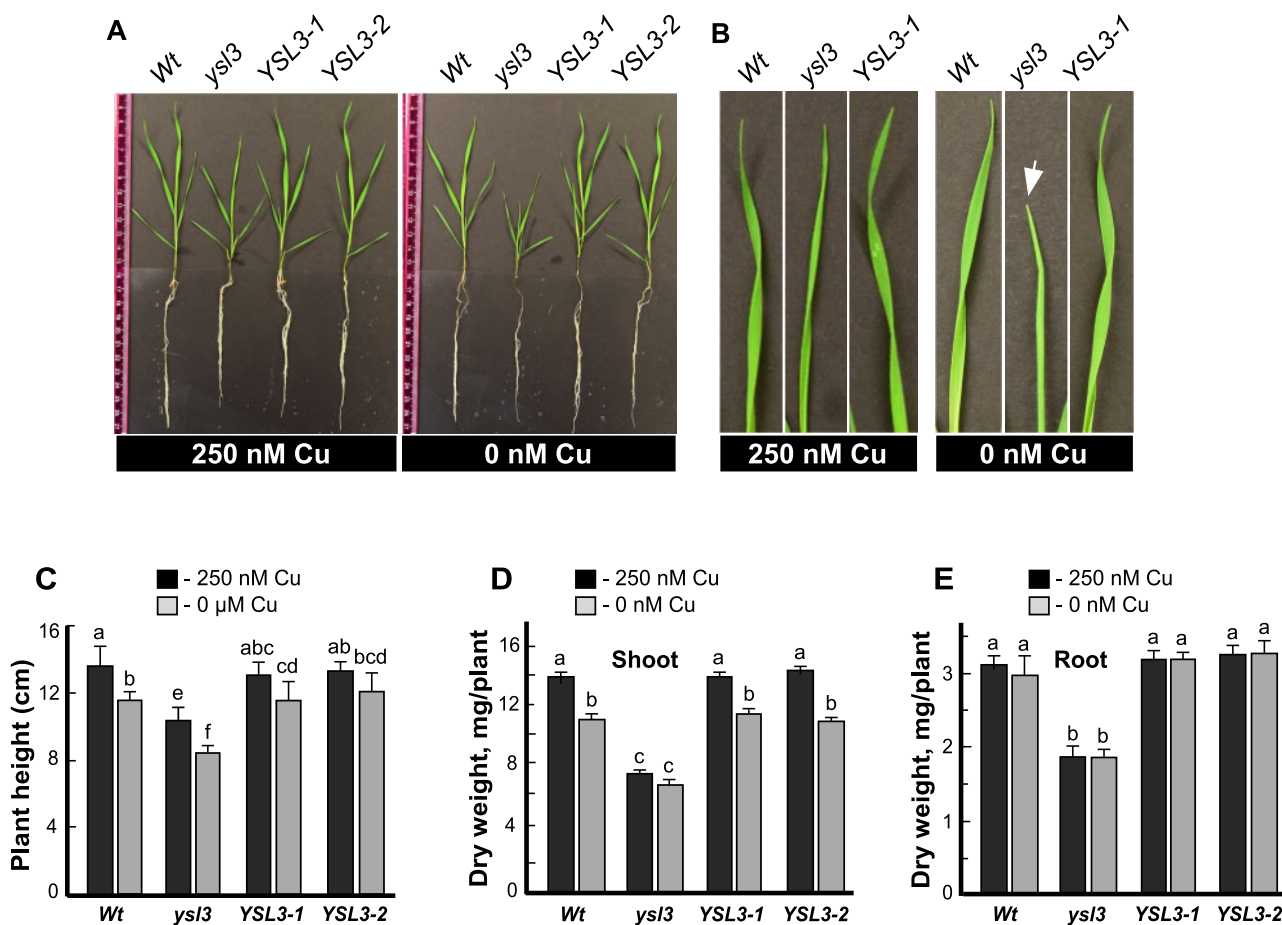


Figure 6 *BdYSL3* is essential for the normal growth of brachypodium under copper deficiency. (A) Wild-type plants (*Wt*), the *ysl3-3* mutant (*ysl3*) and two *ysl3-3* mutant transgenic lines expressing the *BdYSL3* cDNA (*YSL3-1* and *YSL3-2*) were grown hydroponically for three weeks with the indicated concentrations of CuSO_4 . Shown are representative photos from nine plants analyzed per line. Photos were captured after three weeks of growth. (B) Representative images of top (youngest) leaves collected from three-week-old hydroponically grown plants. A white arrow points to a leaf with curled margins. (C) The height, (D, E), the biomass of the brachypodium wild-type plants (*Wt*), *ysl3-3* mutant (*ysl3*) and two *ysl3-3* mutant transgenic lines expressing the *BdYSL3* cDNA (*YSL3-1* and *YSL3-2*) grown hydroponically for three weeks with the indicated concentrations of CuSO_4 . Data in (C–E) show mean values of six independently grown plants from three independent experiments, error bars show SE. Levels not connected by the same letter are significantly different ($p < 0.05$, Tukey-Kramer HSD test).

in development and reproduction. We found that the flowering time of the *ysl3-3* mutant was significantly delayed compared to wild-type plants (Fig. 7A, B). While wild-type plants have started flowering by the 40th d of growth, the *ysl3-3* mutant flowered on average 2 weeks later (Fig. 7A, B). The *ysl3-3* mutant also had shorter flag leaves (Fig. 7C and Table 1) and inflorescences (*alias* spikes) compared to wild-type (Fig. 7C). We then compared the flower development of the *ysl3-3* mutant versus wild-type. Florets in grasses are formed on a structure called spikelet. In brachypodium, a terminal spikelet and a limited number of lateral spikelets give rise to a variable number of florets per spikelet (Derbyshire and Byrne, 2013). We found that while wild-type plants produced two to four lateral spikelets in addition to a terminal spikelet, the *ysl3-3* mutant developed five to seven lateral spikelets in addition to a terminal spikelet (Fig. 7C and Table 1). The increased number of spikelets in the *ysl3-3* mutant resulted in a 1.8-fold increase in the

floret number compared to wild-type plants (Table 1). Fertilizing the *ysl3-3* mutant with 25 μM CuSO_4 functionally complemented the mutant suggesting that the decreased flag leaf length, altered spikelet, and floret formation in the mutant was due to a defect in copper transport (Table 1). Furthermore, the expression of *BdYSL3* cDNA in the *ysl3-3* mutant also functionally complemented the mutant (Fig. 7A–C and Table 1), suggesting that the decreased flag leaf length, altered spikelet, and floret formation in the mutant was due to the loss of *BdYSL3* function.

The *ysl3* mutant has a defect in pollen and floret fertility

Because the *ysl3-3* mutant developed more florets per plant and spike than wild-type (Fig. 7C and Table 1), we anticipated that the mutant would also form more seeds. Surprisingly, there was no difference in grain production per spike between different plant lines (Table 1). Furthermore,

we found a significant (1.8-fold) reduction in floret fertility, as evidenced by a reduced number of grains formed per the number of florets per spike in the mutant versus wild-type (Table 1). Importantly, the expression of *BdYSL3* in the *ysl3-3* mutant or copper supplementation rescued this defect (Table 1). We then examined whether the reduced fertility of the *ysl3-3* mutant is associated with the defect in androecium, gynoecium, or both. We found that pollen viability of *ysl3-3* pollen was nearly half-of observed in the wild-type and fewer *ysl3-3* mutant pollen grains were able to germinate and produce pollen tubes (Fig. 7D, E). We also found that more than 40% of the flowers from *ysl3-3* mutants had altered stigma morphology compared to the wild-type. Specifically, the stigma of the *ysl3-3* mutant appeared more compact and less feathery compared to the wild-type (Fig.

7F). Together, these data suggest that the compromised fertility of the *ysl3-3* mutant might be due to defects in both androecium and gynoecium.

BdYSL3 regulates copper delivery from mature leaves to flag leaves and flowers

We next analyzed copper concentration and spatial distribution in different plant tissues using inductively coupled plasma mass spectrometry (ICP-MS) and 2D synchrotron-X-ray fluorescence (2D-SXRF) microscopy, respectively. We did not find a significant difference in copper concentration in roots of the *ysl3-3* mutant compared to wild-type or *ysl3/YSL3-1* plants (Fig. 8A). However, the *ysl3-3* mutant accumulated 54% more copper in mature leaves compared to wild-type (Fig. 8B). The expression of *BdYSL3* cDNA in the *ysl3-3*

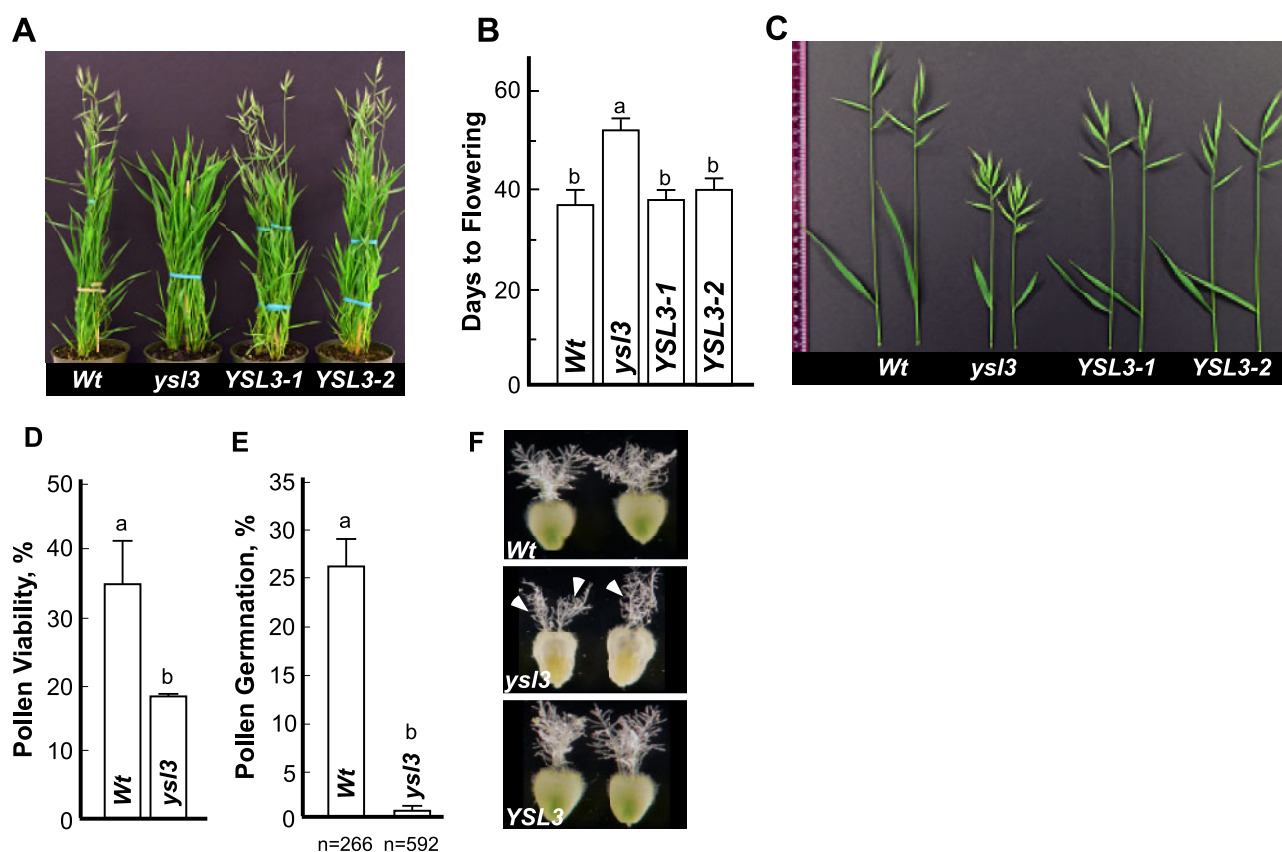


Figure 7 The *ysl3* mutant has a delayed flowering time, altered inflorescence architecture, and pollen viability. The indicated plant lines were grown in soil and fertilized bi-weekly with N–P–K fertilizer. (A) A representative image of the *ysl3-3* mutant, which was still in the vegetative stage in contrast to wild type and *YSL3-1* and *YSL3-2* complementary lines that have reached the reproductive stage of the development. (B) Days to flowering in each of the indicated plant lines. Mean values ± S.E. are shown ($n = 3$ independent experiments with at least six plants analyzed per experiment). Levels not connected by same letter are significantly different ($p < 0.05$, Tukey–Kramer HSD test). (C) A representative image of spikes with a flag leaf collected from plants grown in soil. To collect spikes of all plant lines simultaneously, the *ysl3-3* mutant has been germinated two weeks in advance to other plant lines. (D) The viability of pollen collected from the wild type (*Wt*) and the *ysl3-3* mutant (*ysl3*), grown as described above. Mean values of six independently grown plants from three independent experiments are shown. Error bars show S.E. Levels not connected by same letter are significantly different ($p < 0.05$, Tukey–Kramer HSD test). (E) *In vitro* pollen germination assay shows poor germination rate of the *ysl3-3* mutant compared to wild-type. Values are mean ± S.E. of four and seven independent experiments for wild-type and the *ysl3-3* mutant, respectively; $n =$ number of pollens scored are shown below each bar. Levels not connected by same letter are significantly different ($p < 0.01$, Tukey–Kramer HSD test). (F) The morphology of pistils collected from wild type, the *ysl3-3* mutant, and the *YSL3-1* complementary line, all grown in soil and fertilized bi-weekly with N–P–K. Arrowheads point to stigma sections in the *ysl3-3* mutant that are visibly more compact and less feathery compared to wild type and the *YSL3* complementary line.

Table 1. The *ysl3-3* mutant has altered flower morphology and fertility.

Genotype	Flag leaf length (cm)	Spikelets ^a	Florets ^b	Seeds ^c	Fertile Florets (%)
Wt	7.6 ± 0.23	3.8 ± 0.22	39.8 ± 3.09	29.0 ± 6.71	76.2 ± 1.35
<i>ysl3-3</i>	4.9 ± 0.38*	7.7 ± 0.25*	70.0 ± 4.56*	31.0 ± 0.58	42.6 ± 3.33*
<i>ysl3/YSL3-1</i>	6.4 ± 0.44	4.8 ± 0.48	41.0 ± 2.52	31.3 ± 2.81	75.9 ± 3.76
<i>ysl3</i> + 25 μM CuSO ₄	6.7 ± 0.56	5.0 ± 8.36	46.3 ± 8.36	29.0 ± 3.49	64.8 ± 4.92

Plants were grown in soil and fertilized bi-weekly with a standard N–P–K fertilizer. The *ysl3-3* mutant was also grown in soil and in addition to N–P–K was also fertilized bi-weekly with 25 μM CuSO₄ (*ysl3* + 25 μM CuSO₄). Spikes were collected at the end of the reproductive stage. We note that because the *ysl3-3* mutant is developmentally delayed, its spikes were harvested and fertility was analyzed separately although all plant lines were sown and grown concurrently. Mean values ± SE are shown (*n* = 15 plants per each genotype). Asterisks (*) indicate statistically significant differences from the wild-type (*p* < 0.0001).

^a Spikelets include the terminal spikelet and lateral spikelets.

^b Florets number indicates the total florets produced per spike.

^c Seeds number indicates the total seeds produced per spike.

^d Fertile florets number was calculated as % of seeds formed per the number of florets per spike.

mutant reduced copper accumulation in mature leaves to the wild-type level, suggesting that the observed defects in the *ysl3-3* mutant were due to the loss of BdYSL3 function (Fig. 8B). In contrast to mature leaves, flag leaves and flowers of the *ysl3-3* mutant accumulated 2.9- and 2.6-fold less copper, respectively than corresponding organs of wild-type (Fig. 8C, D). The expression of BdYSL3 in the *ysl3-3* mutant rescued its copper accumulation defect. Together, these results suggested that BdYSL3 might be involved in copper delivery from mature leaves to flag leaves and flowers.

Analysis of mature leaves using 2D-SXRF disclosed that the bulk of copper was associated with leaf veins in both wild-type and the *ysl3-3* mutant (Fig. 9A, B). We also found that copper accumulation was much higher in veins of the *ysl3-3* mutant compared to wild-type (Fig. 9A). Similar to mature leaves, the bulk of copper was associated with major and minor veins of flag leaves in wild-type and the *ysl3-3* mutant (Fig. 9B). However, both vein types in flag leaves of the *ysl3-3* mutant accumulated much less copper compared to the wild-type and the mutant expressing BdYSL3 cDNA (Fig. 9B). The bulk of copper was associated with anthers and ovary of florets in wild-type while copper was barely detectable in anthers and was significantly lower in the ovary of the *ysl3-3* mutant compared to wild-type and the *ysl3-3* mutant expressing BdYSL3 cDNA (Fig. 9C).

We next thought to determine the spatial distribution of copper in nodes because nodes of grasses act as hubs directing and connecting mineral transport pathways for their subsequent distribution to various organs (Yamaji and Ma, 2014). To do so, we utilized 2D-SXRF in a confocal mode (2D-CXRF) using a specialized X-ray collection optic to obtain micron-scale resolution (Mantouvalou et al., 2012; Agyeman-Budu et al., 2016). For the current study, this technique is preferable to traditional SXRF methods (both 2D SXRF and 3D micro-XRF tomography) because it allows comparison of quantitative metal distributions among different samples without the need to control or limit sample thickness or lateral size (Mantouvalou et al., 2012). We found that the bulk of copper was associated with large vascular bundles with a higher concentration in the phloem region in nodes of the wild type (Fig. 9D, E). In contrast, copper accumulation in

vascular bundles was barely detectable in the *ysl3-3* mutant and was mostly associated with the xylem (Fig. 9D, E). Taken together, these data suggested that BdYSL3 might act by loading copper to the phloem and its function is important for copper delivery to flag leaves and reproductive organs, normal flower development, and fertility.

Grains of the *ysl3-3* mutant are smaller, lighter, and accumulate less copper and soluble protein

We next tested whether the loss of the BdYSL3 function also impacts copper accumulation in grains. We found that the concentration of copper in grains of the *ysl3-3* mutant was lower by 44.52% compared to wild-type and the YSL3-1 complementary line (Fig. 10A). This shows that the *ysl3-3* mutant is also defective in copper loading to grains.

While dehusking grains of different plant lines for ICP-MS analysis, we noticed that the *ysl3-3* mutant produced shorter and thinner grains than wild-type plants and both complementary lines. This observation was then confirmed by the analysis of the straight grain length and width (Fig. 10B–D). Consistent with a shorter and thinner size, the 1000-g weight of the *ysl3* mutant was reduced by 30% compared to wild-type (Fig. 10E). The expression of BdYSL3 cDNA in the *ysl3-3* mutant or copper supplementation rescued the grain size and 1000-g weight of the *ysl3-3* mutant. We then compared the concentration of storage proteins in grains of different plant lines. Of three classes of storage proteins (Shewry and Halford, 2002), we analyzed the concentration of saline-extractable proteins corresponding to the albumins/globulins (A/G) fraction. We found that the A/G concentration was significantly lower in grains of the *ysl3-3* mutant compared to wild-type or *ysl3/YSL3* plants. These results show that BdYSL3 function and copper are important for the expression of important agronomic traits including grain size, weight, and protein accumulation.

BdYSL3 is not involved in iron, manganese, and zinc delivery to flowers and grains

We next compared the accumulation of other minerals in different plant lines. We found that iron concentration was 2.3-fold higher in roots of the *ysl3-3* compared to wild-type

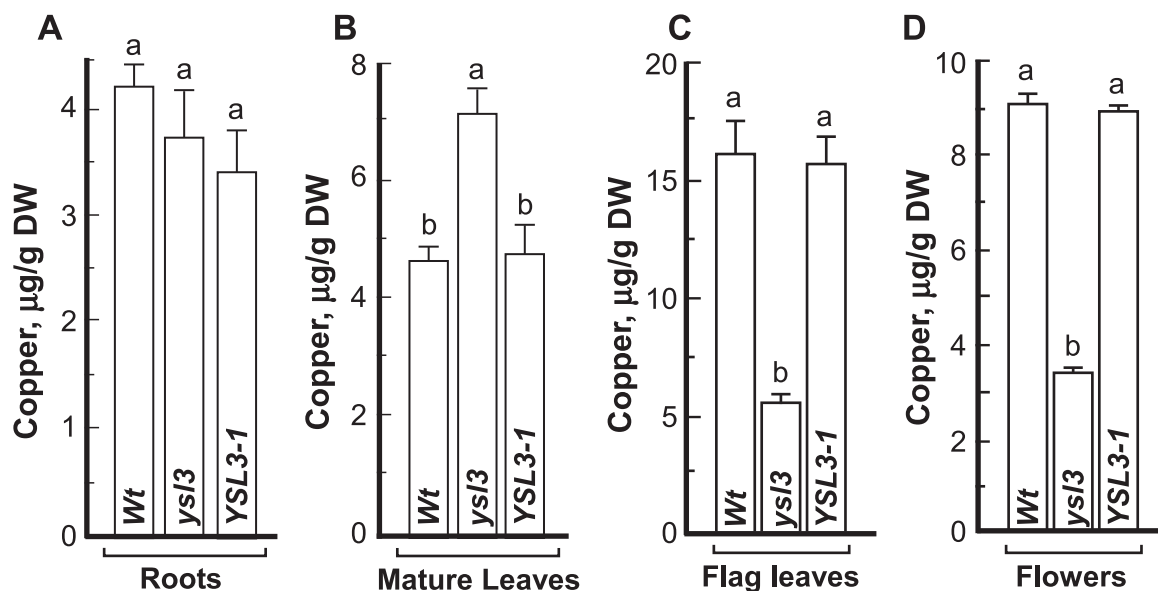


Figure 8 Copper delivery to flag leaves and flowers is impaired in the *ysl3* mutant. ICP-MS-based analysis of the concentration of copper in roots (A), mature (two bottommost) leaves (B), flag leaves (C), and flowers (D) of wild-type plants (Wt), the *ysl3-3* mutant (*ysl3*) and the *ysl3-3* mutant expressing the *YSL3* cDNA (*YSL3-1*). In (A) and (B), plants were grown hydroponically for four weeks with 250 nM CuSO_4 prior to tissue collection. In (C) and (D), tissues were collected from soil grown plants fertilized bi-weekly with N-P-K. (A–D) show mean values \pm S.E. ($n = 3$ independent experiments). Levels not connected by the same letter are significantly different ($p < 0.05$, Tukey–Kramer HSD test). DW, dry weigh.

and was brought back to the level of wild-type by the expression of *BdYSL3* cDNA in the *ysl3-3* mutant (Fig. 11A). Iron accumulation was also higher in mature and flag leaves, but not in flowers of the *ysl3-3* mutant, compared to wild-type and the *ysl3-3* mutant expressing *BdYSL3* cDNA (Fig. 11B, C). SXRF-based imaging did not reveal changes in iron distribution in flag leaves and reproductive organs of the *ysl3-3* mutant compared to wild-type or the *ysl3-3* mutant expressing the *BdYSL3* cDNA (Fig. 11D, E). Consistent with the ICP-MS data (Fig. 11C), iron accumulation was somewhat higher in flag leaves of the *ysl3-3* mutant than the wild-type and the *BdYSL3* complementary line.

Concerning other elements including manganese and zinc, we found that their accumulation was mostly altered in leaves of the *ysl3-3* mutant compared to wild-type and the *BdYSL3* complementary line (Supplemental Figure S6). Importantly, the concentration of iron, zinc, and manganese in flowers and seeds of the *ysl3-3* mutant was similar to that in wild-type and the *BdYSL3* complementary line (Fig. 11C and Supplemental Figure S6). These data show that the decreased flower fertility, and size, weight, and protein accumulation in seeds of the *ysl3-3* mutant are not influenced by iron, manganese or zinc.

Discussion

Copper is important for grain yield in brachypodium and wheat

Providing a sufficient amount of high quality, nutrient-dense food using sustainable and environmentally friendly approaches are among the grand challenges of the 21st century, considering the population growth, the increasing

instances of extreme weather conditions that limit crop yields, and decreasing arable land resources that push the utilization of marginal land for the crop production (Godfray et al., 2010; Ingram and Porter, 2015; Bailey-Serres et al., 2019). Because the micronutrient copper is among yield-limiting factors, here, we sought to determine how copper availability impacts the fertility and yield of a globally important crop, wheat that is also regarded as the most sensitive to copper deficiency. We also aimed to identify copper transporters that are involved in copper delivery to reproductive organs. We found that severe copper deficiency (0 or 10 nM copper) most significantly affected the development of flowers and resulted in a poor grain set in both wheat and its model brachypodium (Fig. 1 and Supplemental Figure 1). Notably, while flowers were formed in both wheat and brachypodium under low copper conditions (50 nM CuSO_4), grain yield was severely affected (Fig. 1E–H). This “silent” effect of copper deficiency on grain set could occur in crops cultivated in agricultural soils with limited copper availability or marginal soils, hence underscoring the need for improving the copper use efficiency of crops for sustainable and environment-friendly crop production.

BdYSL3 is transcriptionally regulated by copper deficiency, expressed in the phloem, and participates in copper delivery to flag leaves and reproductive organs

We next focused on the YSL subfamily of the OPT transporter family because its members have been implicated in the internal transport of micronutrients, including copper (Curie et al., 2008; Yordem et al., 2011). Of the 19 YSL proteins in brachypodium (Schwacke et al., 2003), we selected

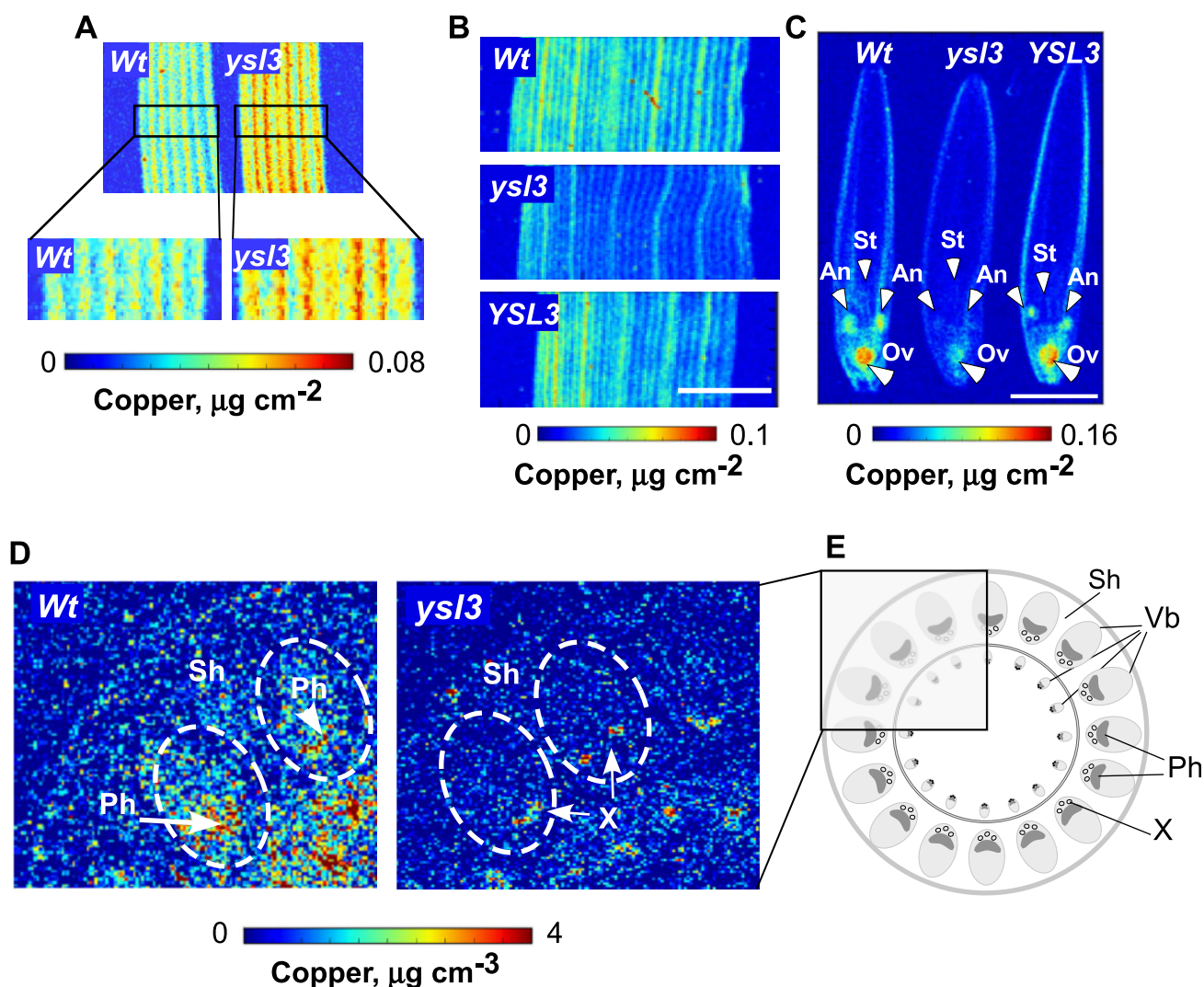


Figure 9 The distribution of copper is altered in the *ysl3-3* mutant. SXRF-based analysis of the spatial distribution of copper in mature leaves (A), flag leaves (B), and florets (C) of the indicated plant lines. Middle part of the leaf was used for SXRF imaging in both (A) and (B). White arrows in (C) point to anthers (An), stigma (S), and ovaries (Ov). Scale bar = 2 mm. Mature leaves in (A) were collected from three-week-old plants, grown hydroponically with $0.25 \mu\text{M}$ CuSO_4 . Flag leaves and florets were collected from soil-grown plants that were fertilized bi-weekly with N–P–K. (D) Two-dimensional confocal SXRF (2D-CSXRF) was used to visualize the spatial distribution of copper in node I of indicated plant lines. (E) illustrates the anatomy of the upper part of the node I. Part of the node in a rectangle was scanned using C-SXRF and is shown in D. Ph, phloem; Sh, leaf sheath; Vb, vascular bundle; Wt, wild type; X, xylem.

BdYSL3 for subsequent studies because its homolog in *A. thaliana*, AtYSL3, is expressed in pollen, is upregulated by copper deficiency in floral organs, acts together with AtYSL1 in mineral nutrient remobilization from senescing tissues and functions in the delivery of micronutrients, including copper, to seeds (Waters et al., 2006; Chu et al., 2010). Furthermore, the BdYSL3 putative ortholog in rice, OsYSL16, is involved in copper distribution to floral organs and its loss-of-function decreases fertility (Zheng et al., 2012; Zhang et al., 2018).

We first showed that under copper sufficiency, BdYSL3 was expressed primarily in leaves. BdYSL3 expression was highly upregulated by copper deficiency in all tissues including roots, mature leaves, flag leaves, and flowers (Fig. 2). The level of BdYSL3 transcript did not change in young leaves

under copper deficiency possibly because its expression in young leaves was already high (Fig. 2). We also showed that the bulk of BdYSL3 expression was associated with the phloem in leaves and node I, although it was also present in mesophyll and phloem parenchyma cells (Fig. 3). Phloem is a vascular tissue that is responsible for the translocation of nutrients including mineral elements from source tissues such as mature leaves to sink tissues including developing flag leaves, flowers, and seeds/grain (White, 2012). Because copper accumulation was significantly higher in mature leaves and significantly lower in flag leaves, flowers, and grains of the *ysl3-3* mutant than that of the wild-type (Figs. 8B–D and 10A), we proposed that BdYSL3 participates in phloem-based copper delivery to sinks. Because copper accumulation was significantly reduced in the phloem and

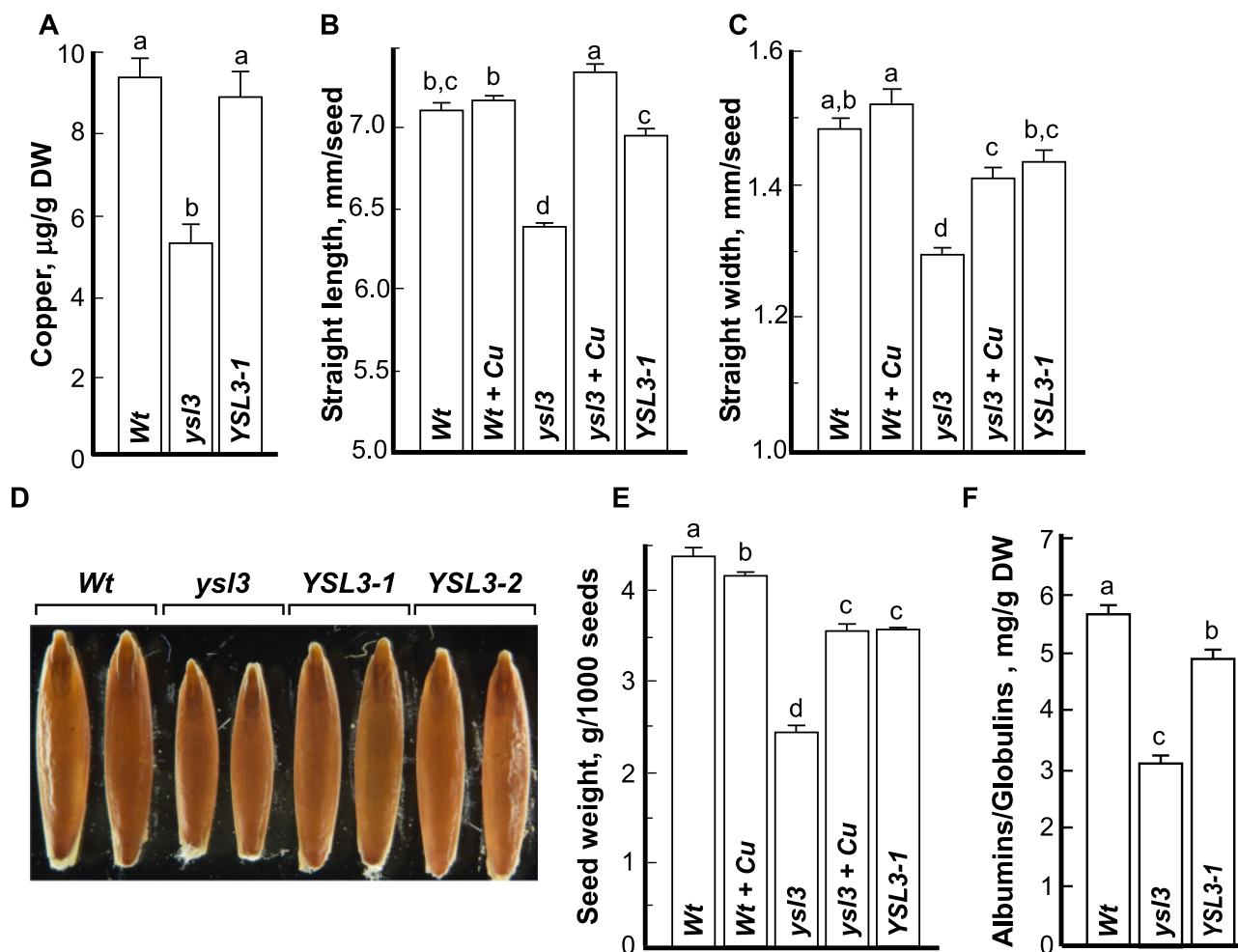


Figure 10 Seeds of the *ysl3-3* mutant accumulate less copper and soluble protein are smaller and lighter. Grains were collected from soil-grown plants that were fertilized bi-weekly with N–P–K. (A) ICP-MS analysis of copper concentration in seeds of the indicated plant lines. (B, C) Straight length and width, respectively, of grains collected from the indicated plant lines. Grains were dehusked and the straight length and width of randomly selected grains were measured using the WinSEEDLETM of STD4800 Scanner (Regent Instruments Inc., Canada, 2015). (D) A representative image of seeds pooled from at least three plants from each independent experiment ($n = 3$). (E, F) The weight of 1,000 dehusked grains and the concentration of soluble proteins in seeds, respectively, in the indicated plant lines. Presented values are arithmetic means \pm S.E. ($n = 3$ pools of seeds from five plants per each line; a representative result from three independent experimental setups is shown). Seeds were pooled together from five plants per line. Levels not connected by same letter are significantly different ($p < 0.05$, Tukey–Kramer HSD test). When indicated (+ Cu), plants were fertilized bi-weekly with $20 \mu\text{M CuSO}_4$. *Wt*, wild-type; *ysl3*, the *ysl3-3* mutant; *YSL3-1*, *YSL3-2*, two transgenic lines of the *ysl3-3* mutant expressing the *YSL3* cDNA; *DW*, dry weight.

remained high in the xylem region in the node 1 of the *ysl3-3* mutant versus wild-type (Fig. 9D), we concluded that *BdYSL3* mediates the loading of copper or copper chelates into the phloem, whereby facilitating copper distribution from source (i.e. mature leaves) to sink tissues (i.e. flag leaves, flowers, grains). It is noteworthy that the ectopic expression of *BdYSL3* in the *ysl3-3* mutant, although functionally complemented the mutant (Figs. 8–10), did not increase copper accumulation in its tissues above the wild-type level. We speculate that *BdYSL3* might be controlled by copper availability not only at the transcript but also protein accumulation level to avoid copper overload as was shown for other transition metal transporters and their regulators, including *Arabidopsis* Iron-regulated Transporter (IRT1) and

the Upstream Regulator of IRT1, URI (Connolly et al., 2002; Barberon et al., 2011; Kim et al., 2019).

***BdYSL3* is downregulated by iron deficiency and the *ysl3-3* mutant accumulates more iron**

We also tested the transcriptional response of *BdYSL3* to iron deficiency because of conflicting reports in the literature regarding the regulation and transport capabilities of its rice homolog, *OsYSL16* (Kakei et al., 2012; Lee et al., 2012; Zheng et al., 2012; Zhang et al., 2018). We found that *BdYSL3* mRNA was significantly downregulated by iron deficiency (Fig. 2C). A similar distinct transcriptional response to copper and iron deficiency was also observed for *AtYSL1* and *AtYSL3* (Waters et al., 2006). We also found that the

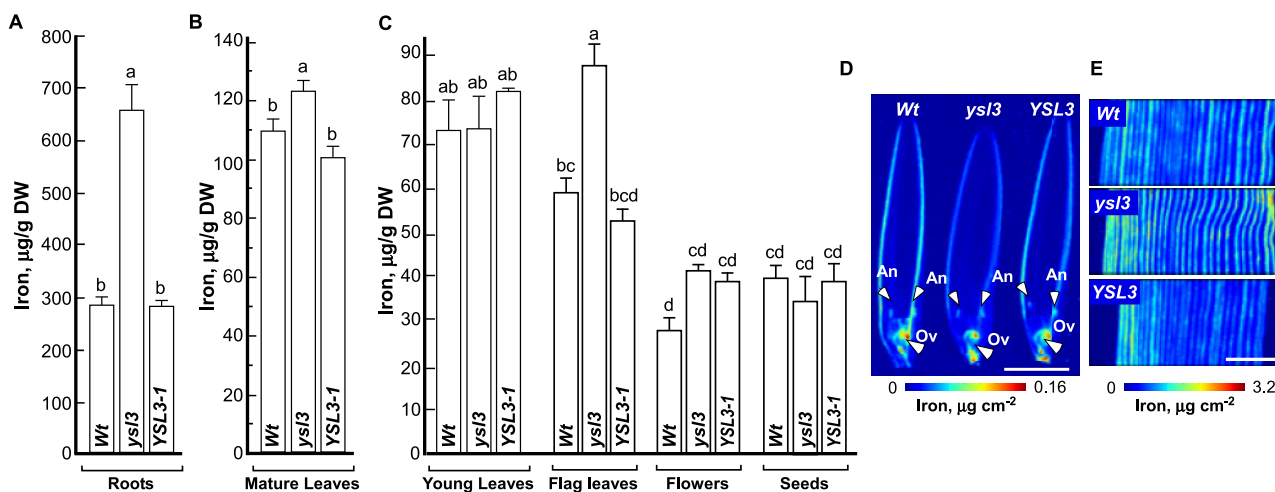


Figure 11 The *ysl3* mutant accumulates more iron in roots, mature and flag leaves and flowers. (A–C) Results from ICP-MS analysis of iron accumulation in the indicated tissues of the indicated plant lines grown as described in legend to Fig. 8. Shown values are arithmetic means \pm S.E. ($n = 3$ independent experiments). Levels not connected by the same letter are significantly different ($p < 0.05$, Tukey–Kramer HSD test). SXRF-based analysis of the spatial distribution of iron in flowers (D) and the middle part of the flag leaf (E). White arrows in (D) point to anthers (An) and ovaries (Ov). Scale bar = 2 mm. Wt, wild-type; *ysl3*, the *ysl3-3* mutant; YSL3-1, the *ysl3-3* mutant expressing the YSL3 cDNA; DW, dry weight.

reduced copper accumulation in roots, flag leaves, and flowers of the *ysl3-3* mutant was associated with the increased accumulation of iron (Figs. 8–11). This was not surprising as crosstalk between copper and iron homeostasis is now well-documented. In fact, low copper accumulation in the *A. thaliana spl7* mutant drives iron accumulation in rosette leaves (Ramamurthy and Waters, 2017) and iron supplementation rescues, in part, growth defects of the copper-deficient *A. thaliana spl7* mutant (Bernal et al., 2012). Because of the similar physicochemical properties of these metals, including similar redox chemistry, their comparable atomic radii, and electrical charges (Doguer et al., 2018), it is tempting to speculate that the increased iron accumulation compensates for the reduced copper concentration in tissues of the *ysl3-3* mutant. In this regard, it has been shown that iron and copper-containing superoxide dismutases (SODs) function equivalently in chloroplasts in scavenging reactive oxygen species, and copper availability is a major determinant of iron SOD expression in *A. thaliana* (Pilon et al., 2011; Ravet and Pilon, 2013).

BdYSL3 localizes to the PM and transports copper ions in *X. laevis* oocytes

YSL proteins from different species localize to different cellular membranes including the PM, chloroplast envelope, or internal cellular membranes (DiDonato et al., 2004; Conte et al., 2013; Divol et al., 2013). We found that BdYSL3 localized to the PM when expressed in *Arabidopsis* protoplasts or in *X. laevis* oocytes (Figs. 4 and 5A). The PM localization of BdYSL3 suggested that this transporter is involved in the influx or efflux of copper or copper–chelate complexes rather than intracellular copper transport.

We next tested the transport capabilities of BdYSL3. It has been shown that YSL transporters are involved in the uptake and the long-distance transport of transition metals

associated with a strong metal-ligand, NA or its derivatives PS such as mugineic acid (MA) and deoxymugenic acid (DMA; Curie et al., 2008). Specifically, the rice protein with closest sequence similarity to BdYSL3, OsYSL16, mediates copper–NA transport in yeast lacking high-affinity copper transporters CTR1p and CTR3p (Zheng et al., 2012). *A. thaliana* YSL2 complements the copper deficiency defect of the yeast CTR1p mutant when copper is supplied in a complex with NA, but not as ionic copper or the copper–MA complex (DiDonato et al., 2004). Electrophysiological studies in *X. laevis* oocytes have shown that maize YS1 transports PS-bound transition metals including copper and NA-bound iron and nickel into oocytes (Schaaf et al., 2004). Thus, we anticipated that BdYSL3 would mediate copper–NA transport as well.

The transport capabilities of BdYSL3 were studied in *X. laevis* oocytes. To our surprise, we found that oocytes expressing BdYSL3 accumulated copper only when it was supplied in ionic form (Fig. 5B, C). Incubation of oocytes with the copper–NA complex did not increase copper accumulation, with uptake levels similar to the mock-expressing cells (Fig. 5C). In contrast, maize YS1 (ZmYS1) mediated the transport of copper–NA into oocytes (Fig. 5C). Interestingly, oocytes expressing ZmYS1 accumulated significantly more copper when it was supplied in the ionic form (Fig. 5C). Based on these results, we concluded that BdYSL3 is capable of transporting free copper ions. In addition, we show that ionic copper was also the preferred transport substrate of the maize YS1 in the heterologous system.

While this transport capability of BdYSL3 and ZmYS1 seems unusual, another member of the OPT family, *A. thaliana* OPT3 has also been shown to transport iron and cadmium ions in the heterologous system (Zhai et al., 2014). Whether BdYSL3 transports copper ions *in planta*, and how its transport capability is coordinated with the function of

other copper ion transporters including members of the COPT and HMA families, and the abundance of copper ligands and chaperons, remains to be elucidated. It is noteworthy, that intracellularly, free copper ions are chelated by copper chaperons that traffic copper through protein–protein interactions from copper transporters at the PM to its destination cuproenzymes or transporters within the cellular compartments (Blaby-Haas et al., 2014; Printz et al., 2016). For example, a copper chaperone, the Antioxidant Protein1 (ATX1) interacts with Cu^{+} -P-type ATPase HMA5 and traffics copper to HMA7/RAN1 in *A. thaliana* (Andres-Colas et al., 2006; Puig et al., 2007; Li et al., 2017). AtHMA5 is involved in Cu^{+} efflux while AtHMA7/RAN7 localizes to the endoplasmic reticulum and is involved in ethylene signaling (Hirayama et al., 1999; Andres-Colas et al., 2006). A plant-specific, Plastid Chaperone 1, PCH1, delivers Cu^{+} to the chloroplast envelope-localized Cu^{+} ATPase PAA1/HMA6, while a Cu^{+} Chaperone for Cu/Zn Superoxide dismutase, CCS, also delivers copper to the thylakoid membrane-localized Cu^{+} ATPase PAA2/HMA8 (Blaby-Haas et al., 2014; Printz et al., 2016).

In addition to copper chaperons, copper chelates including NA, DMA, and the amino acid histidine (His) have been implicated in the long-distance transport of copper via the xylem and the phloem (Printz et al., 2016); small cysteine-rich proteins metallothioneins (MTs) and the ATX1-like Copper Chaperone (CCH) are involved in the phloem-based copper remobilization from source to sink tissues upon senescence (Mira et al., 2001; Benatti et al., 2014; Printz et al., 2016). Because the quadruple MT mutant, *mt1a-2/mt2a-1/mt2b-1/mt3-1* and the *ysl1 ysl3* double mutant of *A. thaliana* lacking YSL1 and YSL3 transporters have a similar defect in copper accumulation in seeds, it was suggested that MTs and YSLs may interact (Printz et al., 2016). It is tempting to speculate that similar protein–protein interactions and copper–ligand exchange reactions occur in trafficking copper to and from BdYSL3 to ensure copper delivery to reproductive organs in brachypodium.

BdYSL3-mediated copper delivery to reproductive organs is important for fertility

Consistent with our past studies of copper distribution in the reproductive organs of *A. thaliana* (Yan et al., 2017), the bulk of copper in florets of brachypodium was associated with anthers of stamens and ovaries of pistils (Fig. 9C). The inability of the *ysl3-3* mutant to deliver copper to these reproductive organs severely reduced pollen viability, germination (Fig. 7D, E) and significantly decreased florets fertility (Table 1). Importantly, copper supplementation or the expression of *BdYSL3* cDNA rescued fertility defects of the *ysl3-3* mutant (Table 1). It is possible that the essential nature of *BdYSL3*-mediated copper delivery to anthers and pistils and the role of copper in pollen fertility stems from its role in maintaining metabolic functions of copper-requiring metalloenzymes and/or for providing respiration-based energy supply for the energy-dependent reproduction

processes via sustaining the function of the copper requiring mitochondrial cytochrome *c* oxidase complex (Denis, 1986; Burkhead et al., 2009). In this regard, *A. thaliana* COX11 homolog is involved in the insertion of copper into the cytochrome *c* oxidase (COX) complex during its assembly in mitochondria, is expressed in germinating pollen among other tissues, and its loss-of-function impairs pollen germination (Radin et al., 2015). We showed recently that copper-deficient *A. thaliana* was infertile, had reduced cytochrome *c* oxidase activity in both leaves and floral buds and accumulated reactive oxygen species in pollen grains (Rahmati Ishka and Vatamaniuk, 2020). It is noteworthy that adequate copper nutrition has also been linked to the successful male fertility in mammals, including humans (Tvrda et al., 2015).

We also noted that copper accumulated in the stigma of pistils of wild-type plants but not of the *ysl3-3* mutant (Fig. 9C) and that the stigma of the *ysl3-3* mutant was more compact and less feathery compared to the wild-type (Fig. 7F). As the receptive portion of the gynoecium, stigma plays an important role in capturing pollen, supporting pollen germination and pollen tube guidance into the style and ovaries (Edlund et al., 2004). Finding that copper is localized to the stigma in brachypodium and that the loss of copper in the stigma of the *ysl3-3* mutant is associated with decreased fertility links stigma development and function to copper homeostasis. In accord with these findings, our recent studies in *A. thaliana* have shown that copper-deficiency abolished stigma papillae development and has led to 100% gynoecium infertility (Rahmati Ishka and Vatamaniuk, 2020). The role of copper in the gynoecium development and fertility is yet to be discovered.

BdYSL3-mediated copper transport is important for the normal transition to flowering and inflorescence architecture

A significant delay in transitioning to reproduction and altered inflorescence architecture, as evidenced by nearly doubled lateral spikelet formation compared to wild-type plants (Fig. 7B, C and Table 1), are intriguing aspects of the *ysl3-3* mutant phenotype. The transition from the vegetative to the reproductive stage and spikelet formation depend on the inflorescence meristem identity and determinacy, the developmental fate of axillary inflorescence meristem, which in turn depends on a variety of environmental and endogenous cues (Barazesh and McSteen, 2008; Pautler et al., 2013; Tanaka et al., 2013; Landrein et al., 2018). For example, shoot apical meristem activity in *A. thaliana* and organogenesis adapt rapidly to changes in nitrate availability in soils through the long-range cytokinin signaling (Landrein et al., 2018). Inflorescence branching and auxiliary inflorescence meristems fates in maize are regulated by sugar metabolism via the function of three RAMOSA genes (Vollbrecht et al., 2005; Bortiri et al., 2006; Satoh-Nagasawa et al., 2006; Claeys et al., 2019). Hormones including auxin and cytokinin are also known to function in inflorescence architecture with

auxin having a critical and conserved role in axillary meristem initiation in *A. thaliana* and maize (Barazesh and McSteen, 2008; Holt et al., 2014). It is noteworthy that copper deficiency in *A. thaliana* also increases shoot branching that is rescued by the exogenous application of auxin or copper (Rahmati Ishka and Vatamaniuk, 2020). In addition to hormones, small non-coding RNA, microRNAs are implicated in developmental transitions and the regulation of inflorescence branching (Holt et al., 2014; D'Ario et al., 2017). Notably, the production of auxin and jasmonic acid is influenced by copper availability and copper deficiency stimulates the production of several miRNA families (Peñarrubia et al., 2015; Pilon, 2017; Yan et al., 2017; Rahmati Ishka and Vatamaniuk, 2020). Considering the prominent role of copper in photosynthesis and the effect of copper homeostasis on hormone or miRNAs production, it is tempting to speculate that the defect in the internal copper distribution and delivery to flag leaves and florets in the *ysl3-3* mutant alters sugar metabolism, and/or miRNA and/or auxin or other hormones production resulting in delayed transition to flowering and altered inflorescence architecture. Because the timing of terminal spikelet differentiation determines the production of lateral spikelets (Bonnett, 1936; Derbyshire and Byrne, 2013), it is also possible that the delayed transition to flowering observed in the *ysl3-3* mutant (Fig. 7A, B) results in increased lateral spikelets production. Although the mutation of the BdYSL3 putative ortholog in rice, OsYSL16, decreases fertility, it does not alter inflorescence architecture (Zhang et al., 2018). The distinct role of orthologous transporters may be related to distinct inflorescence architecture in rice and brachypodium. The rice inflorescence, a panicle, is highly branched and is produced from multiple types of axillary meristems (Kellogg, 2007; Barazesh and McSteen, 2008). The spikelet meristem gives rise to a single floral meristem and a single floret. In contrast, inflorescence in brachypodium is similar to its close relative wheat and is an unbranched spike, where axillary meristems produced by the inflorescence meristem develop directly into spikelets (Bonnett, 1936; Derbyshire and Byrne, 2013). Future studies will determine the specific role of BdYSL3 and copper in determining the inflorescence architecture in brachypodium.

Copper and BdYSL3-mediated copper transport is important for grain size, weight, and soluble proteins accumulation

In addition to decreased fertility, the *ysl3-3* mutant accumulates less copper and soluble protein in grains and its grains are shorter, thinner, and lighter than grains of wild-type, or the *ysl3-3* mutant expressing *BdYSL3* cDNA, or the mutant grown with copper supplementation (Fig. 10). Both grain size and weight are regulated by a complex network that integrates multiple developmental and environmental signals throughout the reproductive stage, and these processes are affected by sink and source characteristics, including the size and photosynthetic capacity of source tissues and the

mobilization of assimilates to the grain (Distelfeld et al., 2014; Li et al., 2018; Brinton and Uauy, 2019). We note that the *ysl3-3* mutant has significantly shorter flag leaves (Fig. 7C and Table 1). Flag leaves are the most efficient functional leaves at the grain filling stage and their size and shape are among the essential traits for the ideal plant-type in crop breeding programs (Li et al., 1998; Zhang et al., 2015). We, therefore, speculate that the decreased grain length, width, and weight in the *ysl3-3* mutant compared to other plant lines are caused, in part, by the reduced source strength of flag leaves which, in turn, is caused by a defect in the BdYSL3-mediated copper distribution to flag leaves, and thus their reduced growth.

It is noteworthy that while manganese and zinc accumulation in leaves of the *ysl3-3* mutant were also altered, the concentration of these metals as well as iron in flowers and seeds was similar to that in wild-type and the *BdYSL3* complementary line (Fig. 11 and Supplementary Figure S6). This finding reinforces the specific role of copper and *BdYSL3* in reproduction and the expression of important agronomic traits including grain size, weight, and protein accumulation.

Grain storage protein accumulation depends on many factors among which are species and genotype variations, as well as environmental conditions, including mineral nutrient availability (Dupont et al., 2006; Engels et al., 2012). Copper deficiency disturbs nitrogen assimilation in legumes, but its implications to nonleguminous plants are less clear (Burkhead et al., 2009). Our survey of publically available RNA-seq data discloses that copper deficiency upregulates putative nitrate transporters in roots and flower buds of *A. thaliana* (Bernal et al., 2012; Yan et al., 2017). However, the connection between copper deficiency and nitrogen/carbon balance is yet to be determined.

In conclusion, this study expands our understanding of the molecular mechanisms of copper transport in crop species, discovers a new avenue of copper function in establishing important agronomic traits, and provides an important step toward the designing of biotechnological strategies aiming for sustainable and environmentally friendly grain yield improvement without the need for chemical fertilization in regions where poor soil quality is a major factor that limits crop productivity.

Materials and methods

Plant materials and growth conditions

Wheat, *T. aestivum* (cv *Bobwhite*), was used for analysis of the effect of copper on growth and reproduction. *B. distachyon* inbred line Bd21-3 regarded as wild-type (Vogel and Hill, 2008) was used for the generation of *BdYSL3* mutant alleles, and transgenic plants expressing *BdYSL3_{pro}-GUS* construct. The *ysl3-3* mutant allele described below was used for transformation to obtain *BdYSL3* complementary lines *YSL3-1* and *YSL3-2*. The generation of *BdYSL3* mutants and other transgenics plants is detailed in the sections below. Depending on the experiment, plants were grown either in soil or hydroponically using procedures described in Jung

et al. (2014). Briefly, after removing lamella and palea, seeds of different plant lines were surface sterilized for 10 min in a solution containing 10% bleach and 0.1% Tween 20 (v/v) and then rinsed five times with deionized H₂O. After the stratification for 24 h at 4°C, seeds were sown in the water-rinsed perlite that was irrigated with 1/2 strength of the hydroponic solution (with or without copper). Seeds were germinated for three days under darkness at 24°C, then transferred to light and grown for five more days. The uniform seedlings were selected and transferred to soil or hydroponic solution. Hydroponic medium for both wheat and brachypodium contained 1 mM KNO₃, 0.5 mM MgSO₄, 1 mM KH₂PO₄, 1 mM Ca (NO₃)₂, 2.5 μM NaCl, 25 μM Fe (III)-HEDTA, 3.5 μM MnCl₂, 0.25 μM ZnSO₄, 0.25 μM CuSO₄, 17.5 μM H₃BO₃, 0.05 μM Na₂MoO₄, and 0.0025 μM CoCl₂ and this medium was replaced weekly. For achieving copper deficiency condition, plants were grown hydroponically for three weeks in a medium lacking copper.

Soil-grown plants were fertilized with the standard N–P–K fertilizer biweekly. To ensure that *BdYSL3* mutant alleles develop and produce seeds, when indicated, 25 μM CuSO₄ was also added to the N–P–K fertilizer. In all cases, plants were grown at 24°C, 20-h-light/18°C, 4-h-dark photoperiod and a photosynthetic flux density of 150 μmol photons m⁻² s⁻¹ light produced with cool-white fluorescent bulbs supplemented by incandescent lighting and 75% relative humidity.

RNA extraction and RT-qPCR analysis

Brachypodium tissues were collected from plants grown either in soil or hydroponically with or without Cu as described above. Because the expression of copper-responsive genes can be affected by the circadian rhythms (Perea-García et al., 2016), samples were collected at a fixed time between 7 and 8 Zeitgeber hour, where the Zeitgeber hour 1 is defined as the first hour of light after the dark period. Two micrograms of total RNA extracted with the TRIzol reagent (Invitrogen) was used as a template for cDNA synthesis with the Affinity Script QPCR cDNA Synthesis Kit (Agilent Technologies). RT-qPCR and data analysis were performed as described in Yan et al. (2017). The expression of *ACTIN2* gene was used for data normalization. Relative expression ($\Delta\Delta C_t$) and fold difference ($2^{-\Delta\Delta C_t}$) were calculated using the CFX Manager Software, version 1.5 (Bio-Rad). The gene-specific primers are listed in Supplemental Table S1.

Plasmid construction for tissue and cellular localization and complementation studies in brachypodium

A set of plasmids was prepared for functional complementation studies, analysis of the tissue-specificity of the expression and subcellular localization of *BdYSL3* in brachypodium, and for the generation of *BdYSL3* knockout plants.

The open reading frame (ORF, 2,115 bp) of *BdYSL3* without a stop codon was PCR-amplified from brachypodium cDNA that was prepared from roots of plants grown hydroponically under control conditions. Three *BdYSL3* isoforms,

Bradi5g17230.1 Bradi5g17230.2, and Bradi5g17230.3 are annotated in the brachypodium genome v3.1 (The International Brachypodium et al., 2010). Because the Bradi5g17230.2 was listed as a prevailing *BdYSL3* isoform, its 2,115 bp ORF was amplified using primer pairs, YSL3-F and YSL3-R (Supplemental Table S1). The primer pairs also included attB sites for cloning of the PCR product by recombination into the entry *pDONR/Zeo* vector (Gehl et al., 2009). The fidelity of the *BdYSL3* transcript was confirmed by sequencing. *pDONR/Zeo-BdYSL3* was then used for recombination cloning into the binary *pSAT6-N1-EGFP-Gate* (Jung et al., 2012) to fuse *BdYSL3* at the C-terminal with EGFP and place it under the control of the cauliflower mosaic virus 35S promoter. The resultant *pSAT6-N1-EGFP-Gate* with or without *BdYSL3* insert was used for the analysis of the subcellular localization of *BdYSL3*-EGFP in protoplasts. To study the tissue and cell-type specificity of *BdYSL3* expression in *Brachypodium*, a putative promoter region of *BdYSL3* (–2207 to –1 bp from the translation initiation codon) was PCR-amplified from *Brachypodium* genomic DNA using primer pairs, *BdYSL3_{pro}*-F and *BdYSL3_{pro}*-R (Supplemental Table S1). The amplified fragments were introduced into the *pDONR/Zeo* entry vector. After confirming the fidelity of *BdYSL3_{pro}* in the *pDONR/Zeo* vector by sequencing, *BdYSL3_{pro}* was transferred by recombination into the Gateway vector, *pMDC164* (Curtis and Grossniklaus, 2003) to fuse *BdYSL3_{pro}* with the bacterial *uidA* gene encoding β-glucuronidase (GUS). *pMDC164* also carries *Escherichia coli* *hptII* gene conferring resistance to hygromycin for the subsequent *in planta* selection.

The design of CRISPR/Cas9 constructs

To generate *BdYSL3* mutant alleles, we used RNA-guided DNA endonuclease system known as CRISPR/Cas9 (CRISPR/CRISPR-associated9 [Cas9] endonuclease; Liu and Fan, 2014). We used monocot-optimized CRISPR/Cas9 vectors that have a modular design allowing multiplexing and targeting different loci within the same gene with different single-guide (sg)RNAs simultaneously to produce larger deletions (Brooks et al., 2014; Čermák et al., 2017). Specifically, we used the module A vector, *pMOD_A1110*, which carries the wheat codon-optimized *Cas9* endonuclease gene under the control of *Zea mays* *Ubi* promoter, modules B and C entry vectors, *pMOD_B2518* and *pMOD_C2518*, respectively for cloning individual sgRNAs under the control of *TaU6* promoter, and the final destination vector, *pTRANS_250d* (Čermák et al., 2017). We designed CRISPR/Cas9 constructs containing two sgRNAs per construct with the intent to create larger deletions within *BdYSL3* coding sequence. Thus, we designed three sgRNAs (sgRNA1, sgRNA2, sgRNA3) within the 5' untranslated region (UTR) and the first exon of *BdYSL3*, respectively (Supplemental Figures 2 and 3). The targeted regions contained the CAS9-recognizing 5'-NGG protospacer adjacent motif (PAM), adjacent to the 20-bp target DNA. The lack of the off-target mutations was confirmed using the CRISPR-P 1.0 web tool (<http://crispr.hzau.edu.cn/CRISPR/> (Lei et al., 2014)). The sgRNA1 and sgRNA2

were separated by 122 bp while sgRNA2 and sgRNA3 were separated by 183 bp (Supplemental Figures 2 and 3). sgRNA oligos were hybridized and annealed prior to cloning into the *Esp31* site of the *pMOD_B2518* (for sgRNA1 or sgRNA2) and *pMOD_C2518* (for sgRNA2 or sgRNA3). The *pMOD_A1110* carrying *TaCas9* and two entry vectors *pMOD_B2518* and *pMOD_C2518* carrying sgRNA1 and 2, respectively or *pMOD_B2518* and *pMOD_C2518* carrying sgRNA2 and 3, respectively were combined by Golden Gate cloning (Weber et al., 2011) with the destination vector, *pTRANS_250d* to generate two CRISPR/Cas9 destination vectors containing with sgRNA1 and sgRNA2 (sgRNAs1 + 2) or sgRNA2 and sgRNA3 (sgRNAs2 + 3); these two vectors were designated *pHS_YSL3(1 + 2)* and *pHS_YSL3(2 + 3)*, respectively.

Agrobacterium tumefaciens-mediated transformation of *B. distachyon*

The *pMDC164* vector containing *BdYLS3_{pro}-GUS*, or *pSATN-EGFP-Gate* vector with *BdYSL3* insert, or CRISPR/Cas 9 vectors, *pHS_YSL3(1 + 2)* and *pHS_YSL3(2 + 3)* were transformed by electroporation into *Agrobacterium tumefaciens* AGL1 strain. All vectors contained the *E. coli hptII* gene conferring resistance to hygromycin for the subsequent *in planta* selection. *Brachypodium* transformation was done as described in Vogel and Hill (2008). Briefly, embryos were dissected from immature seeds of *brachypodium* and placed on callus induction medium (CIM) for seven weeks. The formed callus was then inoculated with *A. tumefaciens* containing a construct of interest. After three days of cocultivation, the callus was transferred to a transformant-selection medium containing 25 µg/mL hygromycin. After six weeks of selection, hygromycin-resistant callus was transferred to the regeneration medium. When plantlets were approximately 5 cm tall, they were transferred to clear tubes with Murashige/Skoog (MS) medium for rooting and the well-rooted plants were transplanted to soil for subsequent genotyping and seed harvesting.

PCR genotyping of CRISPR/Cas9 lines and sequencing

Genomic DNA was extracted from leaves (0.1 g) using a standard cetyl trimethyl ammonium bromide method (Porebski et al., 1997). Twenty-five transgenic T0 lines (13 for *pHZ_YSL3(1 + 2)* and 12 lines for *pHZ_YSL3(2 + 3)*) were PCR-genotyped for the presence of deletions in the *BdYSL3* gene using primer pairs upstream the sgRNA1 (Genotyping-F) and downstream the sgRNA3 (Genotyping-R; Supplemental Table S1). Deletion lines were selected by the band size and plants of the T1 generation of the homozygous deletion lines were re-genotyped for the absence of *Cas9* gene using primer pairs indicated in Supplemental Table S1. Two *Cas9*-free deletion lines per each construct were re-genotyped for the presence of deletion using primer pairs Genotyping F and Genotyping R (Supplemental Table S1). PCR products were loaded onto 1% (w/v) agarose gel,

excised from gel, purifying and cloned into the *pGEM-T Easy* vector (Promega) for sequencing using SP6 and T7 primers. DNA sequencing results were analyzed against the *brachypodium* genome v3.1 (The International *Brachypodium* et al., 2010). Sequence alignments were done using DNAMAN software.

Tissue- and cell-type specificity of *BdYSL3* expression

Brachypodium Bd21-3 inbred line was transformed with *pMDC164* vector-containing *BdYLS3_{pro}-GUS*. Five out of the 13 independent transgenic lines (T1 generation) were used for GUS staining. Samples, collected from plants grown hydroponically with or without copper were fixed in 90% acetone on ice for 15 min. After washing thoroughly with ddH₂O, samples were incubated at 37°C overnight in GUS staining solution containing 1 mM K₃[Fe(CN)₆], 1 mM 5-bromo-4-chloro-3-indolyl-β-D-glucuronide (X-Gluc), 100 mM sodium phosphate buffer (pH 7.0), 10 mM Na₂EDTA, and 0.1% (v/v) TritonX-100 (Inoue et al., 2003). After staining, samples were soaked five times (3–4 h each time) in 90% ethanol to remove chlorophyll that interferes with observation of the blue GUS stain. Hand-cut sections were prepared from stems using a feather double-edge razor blade. Staining patterns were analyzed using the Zeiss 2000 stereomicroscope. Images were collected using a Canon PowerShot S3 IS digital camera and a CS3IS camera adapter. Images were processed using the Adobe Photoshop software package, version 12.0.

Functional complementation assays in the *Brachypodium ysl3-3* mutant

The *pSATN-EGFP-Gate* vector containing the *BdYSL3* cDNA insert was transformed into the *ysl3-3* mutant allele using the described above *Agrobacterium*-mediated transformation. Two independent transgenic lines, *YSL3-1* and *YSL3-2* were selected for functional complementation assays. For plants growing hydroponically, four-week-old plants were imaged prior to tissue harvesting and biomass analysis. For plants grown in soil, days from germination to flowering were recorded for each genotype. Spike phenotypes were photographed. The floret number was estimated when seeds were ready for harvesting. The fertility was calculated as number of filled seeds per number of florets. Seed weight was measured from 1,000 seeds per each line.

The subcellular localization of *BdYSL3* in *A. thaliana* protoplasts

To study the subcellular localization of *BdYSL3*, *pSATN-EGFP-Gate* vector with or without *BdYSL3* cDNA insert was transfected into *A. thaliana* protoplasts by a polyethylene glycol-mediated method as described (Zhai et al., 2009). EGFP-mediated fluorescence and chlorophyll autofluorescence were visualized using FITC (for EGFP) or rhodamine (for chlorophyll) filter sets of the Axio Imager M2 microscope equipped with the motorized Z-drive (Zeiss).

Images were obtained using the high-resolution 25 AxioCam MR Camera and processed using the Adobe Photoshop software package, version 12.0.

BdYSL3 expression in *Xenopus leavis* oocytes for cellular localization and transport assays

The coding sequence of *BdYSL3* was amplified and cloned into *Xenopus* oocyte expression vectors (with and without N-terminus YFP) by the advanced uracil excision-based cloning technique described previously in (Nour-Eldin et al., 2006). The pOO2 plasmid carrying *ZmYS* cDNA was a generous gift from Profs. Nicolaus von Wiren and Uwe Ludewig (The Leibniz Institute of Plant Genetics and Crop Research, University of Hohenheim, Germany, respectively). pOO2-*ZmYS* is described in Schaaf et al. (2004). cRNAs were synthesized using the T7 and SP6 mMessage mMachine in vitro transcription kit following the manufacturer's guidelines.

Stage V and VI oocytes harvesting, defolliculation, and incubations were performed as described earlier (Zhai et al., 2014). All animal procedures were performed in accordance with Cornell University IACUC Protocol number 2017-0139. Oocytes were injected with 50 nL water (control) or 50 nL of water containing 50 ng of *BdYSL3*, *ZmYS* or YFP::*BdYSL3* cRNA. Cells were incubated in ND96 solution at 18°C for four days prior to the cellular localization and uptake assays.

Preparation of the copper–NA complex

The stock solution of copper–nicotianamine (Cu–NA, 500 μM) was prepared as described (Schaaf et al., 2004; Zheng et al., 2012). Briefly, NA (Santa Cruz[®] Biotechnology), dissolved in 10 mM Mes-Tris buffer (pH 7.0) was mixed with CuSO₄ in 1.5–1.0 of NA to CuSO₄ ratio in a buffer containing 10 mM Mes-Tris, pH 7.0. The mixture was incubated at 65°C for 10 min.

Cellular localization of YFP::BdYSL3 chimera in *X. oocytes*

The YFP signal of the expressed chimera was detected on a confocal laser-scanning microscope (TCS SP5, Leica). A PM stain (CellMaskTM Plasma Membrane Stains, Deep Red C10064, Thermo Fisher Scientific, USA) was used as a marker for PM co-localization. The YFP was excited with the 514 nm line (Argon laser gain: 40%) and the emission signal was collected between 524 to 566 nm (PMT gain: 115). The Deep Red stain was excited with the 594 nm line (Helium Neon laser gain: 35%) and the emission signal was collected between 614 and 708 nm (PMT gain: 26).

Metal uptake into *BdYSL3* expressing oocytes

The basal uptake solution consisted of a modified ND96 solution containing 96 mM NaCl, 1 mM KCl, 0.9 mM CaCl₂, buffered with 5 mM 2-(N-morpholino) ethanesulfonic acid/NaOH to pH 6.0, as previous studies determined these conditions were suitable to minimize endogenous transport in oocytes (Zhai et al., 2014). The uptake solutions were supplemented with 100 μM Cu–NA

or 100 μM CuSO₄. At a given time point, the uptake was terminated by washing oocytes through six consecutive ice-cold basal uptake solution. Each sample consisted of 8–10 oocytes, with 5 replicates per data point. Samples were digested in 100 μL of 70% HClO₄, resuspended in 5 mL of 0.1 M nitric acid, and analyzed using inductively coupled plasma mass spectrometry (Sciex ICP-MS). Uptake data are expressed “per oocyte” and are representative of three independent experiments.

Elemental analysis

Elemental analysis was performed using inductively coupled plasma mass spectrometry (ICP-MS) as described in Yan et al. (2017). Briefly, for analysis of metal concentration in roots and young leaves, plants were grown hydroponically as described above. Root tissues were collected and desorbed in 10 mM EDTA for 5 min followed by washing in a solution of 0.3 mM BPS and 5.7 mM sodium dithionite for 10 min before rinsing three times with deionized water. For the analysis of metal concentration in flag leaves, flowers and seeds, plant lines were grown in soil. The metal concentration was determined by ICP-MS (Agilent 7700) after diluted to 10 mL with deionized water.

Synchrotron X-ray fluorescence (SXRF) microscopy

Two-dimensional synchrotron X-ray fluorescence microscopy imaging the spatial distribution of copper in fresh tissues, including leaves and flowers was done at the F3 station at the Cornell High Energy Synchrotron Source (CHESS). Imaging of copper distribution in nodes was done using two-dimensional confocal SXRF (2D-CXRF) at beamline 5-ID (SRX) of National Synchrotron Light Source (NSLS). A detailed description of procedures is provided in the [Supplementary Information](#).

Extraction and quantification of soluble proteins

Soluble fraction of proteins (albumins/globulins [A/G]) was analyzed as described in Wieser et al. (1998). Briefly, grains were collected from soil-grown plants that were fertilized bi-weekly with N–P–K. Proteins were extracted from 100 mg of finely ground seeds by shaking for 20 min at room temperature in a 67 mM phosphate buffer (pH 7.6) containing 0.4 M NaCl. The suspension was cleared by centrifugation at 6000 × g for 15 min and the supernatant was transferred to a fresh tube. The extraction procedure was repeated two more times. Supernatants from three extractions were combined and soluble proteins were quantified using Non-Interfering Protein Assay Kit (Geno Technology, St Louis, MO, USA).

Pollen viability assays

Plants were grown in soil as described above. Pollen viability was analyzed using double staining with fluorescein diacetate and propidium iodide as described (Mandaokar and Browse, 2009). Briefly, fluorescein diacetate (2 mg/mL) was prepared in acetone and added drop by drop into 17% sucrose. Propidium iodide (1 mg/mL made in water) was

diluted to a final concentration of 100 $\mu\text{g}/\text{mL}$ with 17% sucrose (w/v). Anthers were dissected from flowers under the stereo microscope and pollen was released by tapping into the Eppendorf tube containing fluorescein diacetate and propidium iodide solutions mixed in 1:1 ratio prior to fluorescence microscopy. Pollens were imaged under the Axio Imager M2 microscope (Zeiss, Inc) using FITC and Texas red filter sets to visualize fluorescein- and propidium iodide-mediated fluorescence. Viable pollen was stained green because live cells uptake fluorescein diacetate and convert it to fluorescein, which emits blue–green light under UV irradiation (Heslop-Harrison and Heslop-Harrison, 1970). Unviable pollen was red because while propidium iodide is excluded from living cells, it labels dead cells with red–orange fluorescence under UV irradiation (Regan and Moffatt, 1990). The number of viable and aborted pollens was counted in 10 sample microscope fields in each of three independent experiments. Images were collected with the high-resolution AxioCam MR camera and processed using the Adobe Photoshop software package, version 12.0.

Pollen germination assays

Florets, collected from soil-grown plants, were incubated for 1 h at 4°C prior to anther dissection and pollen collection. Pollen was germinated in the medium containing 1 mM CaCl_2 , 1 mM KCl, 0.8 mM MgSO_4 , 1.6 mM H_3BO_3 , 30 μM CaSO_4 , 0.03% casein, 0.3% MES, 10% sucrose, and 12.5% polyethylene glycol (Zhang et al., 2018). Germination was scored after 3–4 h of incubation at 24°C.

Statistical analysis

All the presented data are the mean values of three independent experiments. SPSS 20.0 (SPSS, Chicago, IL, USA) and JMP Pro 14.0.0 (SAS) was utilized for statistical analyses. Comparison of the means for all pairs was done using Tukey–Kramer HSD test of one-way ANOVA at a significance level of $p < 0.05$, unless specified otherwise.

Accession numbers

Sequence data from this article can be found in the GenBank/EMBL libraries under the following accession numbers (accession numbers in parenthesis): *BdYSL3* (BRADI_5g17230v3); *BdACT2* (BRADI_1g10630v3); *OsYSL16* (LOC4336546); *ZmYS1* (GRMZM2G156599); *AtYSL3* (AT5G53550); *AtYSL1* (AT4G24120); *AtSPL7* (AT5G18830); *AtCITF1* (AT1G71200); *AtOPT3* (AT4G16370); *AtHMA5* (AT1G63440); *AtHMA6* (AT4G33520); *AtHMA7* (AT5G44790); *AtHMA8* (AT5G21930); *AtATX1* (AT1G66240); *AtCCS* (AT1G12520); *AtCCH* (AT3G56240); *AtCOX11* (AT1G02410); *AtIRT1* (AT4G19690); *AtURI* (AT3G19860).

Supplemental data

Supplemental Figure S1. Copper deficiency affects flower development and reduces tiller and head number in wheat and brachypodium.

Supplemental Figure S2. Generation of CRISPR/Cas9 mutant alleles for *YSL3*.

Supplemental Figure S3. The genomic DNA sequence of *YSL3* that was used for designing sgRNAs.

Supplemental Figure S4. RT-qPCR analysis of *YSL3* transcript abundance in roots and leaves of *Brachypodium* wild-type (*Wt*), the *ysl3-3* mutant (*ysl3*) and two *ysl3-3* mutant transgenic lines expressing the *BdYSL3* cDNA (*YSL3-1*; *YSL3-2*).

Supplemental Figure S5. The *ysl3-3* mutant is not sensitive to iron, manganese or zinc deficiency.

Supplemental Figure S6. The accumulation of zinc and manganese is not altered in seeds of the *ysl3-3* mutant.

Supplemental Table S1. A list of used oligos.

Supplemental Results.

Supplemental Methods.

Supplemental References.

Acknowledgements

We would like to thank Professor Mark Sorrells and Ellie Taagen (Cornell University, USA) for providing *T. aestivum* seeds and for assisting in using the WinSEEDLETM of STD4800 Scanner. pOO2 plasmid carrying *ZmYS* cDNA was a generous gift from Prof. Nicolaus von Wiren (The Leibniz Institute of Plant Genetics and Crop Research, Germany) and Prof. Uwe Ludewig (University of Hohenheim, Germany). We would like to thank Haoyu Lin for help in phenotyping wheat; 2D-CXRF experiments used resources of the National Synchrotron Light Source II, a U.S. Department of Energy (DOE) Office of Science User Facility operated for the DOE Office of Science by Brookhaven National Laboratory under Contract No. DE-SC0012704. Non-confocal 2D-XRF measurements were conducted at the Cornell High Energy Synchrotron Source (CHESS) which during the period of research was supported by the National Science Foundation under award DMR-1332208. Custom optics for 2D-CXRF experiments were fabricated at the Cornell NanoScale Facility, an NNCI member supported by NSF Grant NNCI-2025233. We thank John Grazul at the Cornell Center for Materials Research (CCMR) for assisting in preparation samples for 2D-CXRF. CCMR facility is supported by the National Science Foundation under Award Number DMR-1719875. H. S. and Y. J. were supported in part by National Natural Science Foundation of China (#31301349, 30870154, 30901052, 30900087) to H. Z. and Y. Z. and The Schwartz Research Fund for Women in Life Sciences awarded to O. K. V. This study was funded by the Agriculture and Food Research Initiative Awards # 2018-67013-27418 and 2021-67013-33798 from the USDA National Institute of Food and Agriculture; NSF-IOS #1656321 to O. K. V., and CRDF-GLOBAL U.S.–Ukraine Competition OISE-9531011, awarded to O. K. V., O. I. T and N. D. R.

Conflict of interest statement. The authors declare no conflict of interest.

References

Abdel-Ghany SE, Müller-Moulé P, Niyogi KK, Pilon M, Shikanai T (2005) Two P-type ATPases are required for copper

- delivery in *Arabidopsis thaliana* chloroplasts. *The Plant Cell* **17**: 1233–1251
- Agyeman-Budu DN, Choudhury S, Coulthard I, Gordon R, Hallin E, Woll AR** (2016) Germanium collimating micro-channel arrays for high resolution, high energy confocal X-ray fluorescence microscopy. *Icxom23: International Conference on X-Ray Optics and Microanalysis* **1764**.
- Andres-Colas N, Sancenon V, Rodriguez-Navarro S, Mayo S, Thiele DJ, Ecker JR, Puig S, Penarrubia L** (2006) The *Arabidopsis* heavy metal P-type ATPase HMA5 interacts with metallochaperones and functions in copper detoxification of roots. *Plant J* **45**: 225–236
- Bailey-Serres J, Parker JE, Ainsworth EA, Oldroyd GED, Schroeder JI** (2019) Genetic strategies for improving crop yields. *Nature* **575**: 109–118
- Barazesh S, McSteen P** (2008) Hormonal control of grass inflorescence development. *Trends in Plant Science* **13**: 656–662
- Barberon M, Zelazny E, Robert S, Conéjéro G, Curie C, Friml J, Vert G** (2011) Monoubiquitin-dependent endocytosis of the iron-regulated transporter 1 (IRT1) transporter controls iron uptake in plants. *Proc Natl Acad Sci U S A* **108**: E450–E458
- Benatti MR, Yookongkaew N, Meenam M, Guo WJ, Punyasuk N, AbuQamar S, Goldsbrough P** (2014) Metallothionein deficiency impacts copper accumulation and redistribution in leaves and seeds of *Arabidopsis*. *New Phytologist* **202**: 940–951
- Bernal M, Casero D, Singh V, Wilson GT, Grande A, Yang H, Dodani SC, Pellegrini M, Huijser P, Connolly EL, et al.** (2012) Transcriptome sequencing identifies SPL7-regulated copper acquisition genes FRO4/FRO5 and the copper dependence of iron homeostasis in *Arabidopsis*. *The Plant Cell Online* **24**: 738–761
- Blaby-Haas CE, Padilla-Benavides T, Stübe R, Argüello JM, Merchant SS** (2014) Evolution of a plant-specific copper chaperone family for chloroplast copper homeostasis. *Proc Natl Acad Sci* **111**: E5480–E5487
- Bonnett OT** (1936) The development of the wheat spike. *J Agricul Res* **53**: 0445–0451
- Bortiri E, Chuck G, Vollbrecht E, Rocheford T, Martienssen R, Hake S** (2006) *ramosa2* encodes a lateral organ boundary domain protein that determines the fate of stem cells in branch meristems of maize. *Plant Cell* **18**: 574–585
- Brinton J, Uauy C** (2019) A reductionist approach to dissecting grain weight and yield in wheat. *J Integrat Plant Biol* **61**: 337–358
- Broadley M, Brown P, Cakmak I, Rengel Z, Zhao F** (2012) Chapter 7—Function of nutrients: Micronutrients A2—Marschner, Petra. In *Marschner's Mineral Nutrition of Higher Plants (Third Edition)*. Academic Press, San Diego, pp 191–248
- Brooks C, Nekrasov V, Lippman ZB, Van Eck J** (2014) Efficient gene editing in tomato in the first generation using the clustered regularly interspaced short palindromic repeats/CRISPR-associated9 system. *Plant Physiol* **166**: 1292–1297
- Burkhead JL, Gogolin Reynolds KA, Abdel-Ghany SE, Cohu CM, Pilon M** (2009) Copper homeostasis. *New Phytologist* **182**: 799–816
- Čermák T, Curtin SJ, Gil-Humanes J, Čegan R, Kono TJY, Konečná E, Belanto JJ, Starker CG, Mathre JW, Greenstein RL, et al.** (2017) A multipurpose toolkit to enable advanced genome engineering in plants. *The Plant Cell* **29**: 1196–1217
- Chu HH, Chiecko J, Punshon T, Lanzirrotti A, Lahner B, Salt DE, Walker EL** (2010) Successful reproduction requires the function of *Arabidopsis* Yellow Stripe-Like1 and Yellow Stripe-Like3 metal-nicotianamine transporters in both vegetative and reproductive structures. *Plant Physiol* **154**: 197–210
- Claeys H, Vi SL, Xu X, Satoh-Nagasawa N, Eveland AL, Goldshmidt A, Feil R, Beggs GA, Sakai H, Brennan RG, et al.** (2019) Control of meristem determinacy by trehalose 6-phosphate phosphatases is uncoupled from enzymatic activity. *Nature Plants* **5**: 352–357
- Connolly EL, Fett JP, Guerinot ML** (2002) Expression of the IRT1 metal transporter is controlled by metals at the levels of transcript and protein accumulation. *The Plant Cell* **14**: 1347–1357
- Conte SS, Chu HH, Rodriguez DC, Punshon T, Vasques KA, Salt DE, Walker EL** (2013) *Arabidopsis thaliana* Yellow Stripe1-Like4 and Yellow Stripe1-Like6 localize to internal cellular membranes and are involved in metal ion homeostasis. *Front Plant Sci* **4**: 283–283
- Curie C, Cassin G, Couch D, Divol F, Higuchi K, Le Jean M, Misson J, Schikora A, Czernic P, Mari S** (2008) Metal movement within the plant: contribution of nicotianamine and yellow stripe 1-like transporters. *Ann Botany* **103**: 1–11
- Curtis MD, Grossniklaus U** (2003) A gateway cloning vector set for high-throughput functional analysis of genes in planta. *Plant Physiol* **133**: 462–469
- D'Ario M, Griffiths-Jones S, Kim M** (2017) Small RNAs: big impact on plant development. *Trends Plant Sci* **22**: 1056–1068
- Denis M** (1986) Structure and function of cytochrome-c oxidase. *Biochimie* **68**: 459–470
- Derbyshire P, Byrne M** (2013) MORE SPIKELETS1 is required for spikelet fate in the inflorescence of *Brachypodium distachyon*. *Plant Physiology* **161**: 1291–1302
- DiDonato RJ, Roberts LA, Sanderson T, Eisley RB, Walker EL** (2004) *Arabidopsis* Yellow Stripe-Like2 (YSL2): a metal-regulated gene encoding a plasma membrane transporter of nicotianamine--metal complexes. *Plant J* **39**: 403–414
- Distelfeld A, Avni R, Fischer AM** (2014) Senescence, nutrient remobilization, and yield in wheat and barley. *J Exp Botany* **65**: 3783–3798
- Divol F, Couch D, Conéjéro G, Roschttardt H, Mari S, Curie C** (2013) The *Arabidopsis* YELLOW STRIPE LIKE4 and 6 transporters control iron release from the chloroplast. *Plant cell* **25**: 1040–1055
- Doguer C, Ha J-H, Collins JF** (2018) Intersection of iron and copper metabolism in the mammalian intestine and liver. *Comprehens Physiol* **8**: 1433–1461
- Dupont FM, Hurkman WJ, Vensel WH, Tanaka C, Kothari KM, Chung OK, Altenbach SB** (2006) Protein accumulation and composition in wheat grains: effects of mineral nutrients and high temperature. *Eur J Agron* **25**: 96–107
- Edlund AF, Swanson R, Preuss D** (2004) Pollen and stigma structure and function: the role of diversity in pollination. *Plant Cell* **16**: S84–S97
- Engels C, Kirkby E, White P** (2012) Chapter 5—mineral nutrition, yield and source-sink relationships. In *P Marschner, ed, Marschner's Mineral Nutrition of Higher Plants (Third Edition)*. Academic Press, San Diego, pp 85–133
- Gayomba SR, Jung HI, Yan J, Danku J, Rutzke MA, Bernal M, Kramer U, Kochian LV, Salt DE, Vatamaniuk OK** (2013) The CTR/COPT-dependent copper uptake and SPL7-dependent copper deficiency responses are required for basal cadmium tolerance in *A. thaliana*. *Metallomics* **5**: 1262–1275
- Gehl C, Waadt R, Kudla J, Mendel RR, Hansch R** (2009) New GATEWAY vectors for high throughput analyses of protein-protein interactions by bimolecular fluorescence complementation. *Mol Plant* **2**: 1051–1058
- Godfray HCJ, Beddington JR, Crute IR, Haddad L, Lawrence D, Muir JF, Pretty J, Robinson S, Thomas SM, Toulmin C** (2010) Food security: the challenge of feeding 9 billion people. *Science* **327**: 812–818
- Graham RD** (1978) Tolerance of triticale, wheat and rye to copper deficiency. *Nature* **271**: 542–543
- Heslop-Harrison J, Heslop-Harrison Y** (1970) Evaluation of pollen viability by enzymatically induced fluorescence; intracellular hydrolysis of fluorescein diacetate. *Stain Technol* **45**: 115–120
- Hirayama T, Kieber JJ, Hirayama N, Kogan M, Guzman P, Nourizadeh S, Alonso JM, Dailey WP, Dancis A, Ecker JR** (1999) RESPONSIVE-TO-ANTAGONIST1, a Menkes/Wilson disease-related

- copper transporter, is required for ethylene signaling in *Arabidopsis*. *Cell* **97**: 383–393
- Holt AL, van Haperen JMA, Groot EP, Laux T** (2014) Signaling in shoot and flower meristems of *Arabidopsis thaliana*. *Curr Opin Plant Biol* **17**: 96–102
- Ingram JSI, Porter JR** (2015) Plant science and the food security agenda. *Nature Plants* **1**: 15173
- Inoue H, Higuchi K, Takahashi M, Nakanishi H, Mori S, Nishizawa NK** (2003) Three rice nicotianamine synthase genes, OsNAS1, OsNAS2, and OsNAS3 are expressed in cells involved in long-distance transport of iron and differentially regulated by iron. *Plant Journal* **36**: 366–381
- Jung H-i, Gayomba S, Yan J, Vatamaniuk OK** (2014) *Brachypodium distachyon* as a model system for studies of copper transport in cereal crops. *Front Plant Sci* **5**: 236–240
- Jung H-i, Gayomba SR, Rutzke MA, Craft E, Kochian LV, Vatamaniuk OK** (2012) COPT6 is a plasma membrane transporter that functions in copper homeostasis in *Arabidopsis* and is a novel target of SQUAMOSA promoter-binding protein-like 7. *J Biol Chem* **287**: 33252–33267
- Jung HI, Gayomba SR, Rutzke MA, Craft E, Kochian LV, Vatamaniuk OK** (2012) COPT6 is a plasma membrane transporter that functions in copper homeostasis in *Arabidopsis* and is a novel target of SQUAMOSA promoter-binding protein-like 7. *J Biol Chem* **287**: 33252–33267
- Kakei Y, Ishimaru Y, Kobayashi T, Yamakawa T, Nakanishi H, Nishizawa NK** (2012) OsYSL16 plays a role in the allocation of iron. *Plant Mol Biol* **79**: 583–594
- Kampfenkel K, Kushnir S, Babiyshuk E, Inze D, Van Montagu M** (1995) Molecular characterization of a putative *Arabidopsis thaliana* copper transporter and its yeast homologue. *J Biol Chem* **270**: 28479–28486
- Kellogg EA** (2007) Floral displays: genetic control of grass inflorescences. *Curr Opin Plant Biol* **10**: 26–31
- Kim SA, LaCroix IS, Gerber SA, Guerinot ML** (2019) The iron deficiency response in *Arabidopsis thaliana* requires the phosphorylated transcription factor URI. *Proc Natl Acad Sci U S A* **116**: 24933–24942
- Landrein B, Formosa-Jordan P, Malivert A, Schuster C, Melnyk CW, Yang W, Turnbull C, Meyerowitz EM, Locke JCW, Jönsson H** (2018) Nitrate modulates stem cell dynamics in *Arabidopsis* shoot meristems through cytokinins. *Proc Natl Acad Sci* **115**: 1382–1387
- Lee S, Ryoo N, Jeon J-S, Guerinot ML, An G** (2012) Activation of rice Yellow Stripe1-Like 16 (OsYSL16) enhances iron efficiency. *Molecules and cells* **33**: 117–126
- Lei Y, Lu L, Liu H-Y, Li S, Xing F, Chen L-L** (2014) CRISPR-P: a web tool for synthetic single-guide RNA design of CRISPR-system in plants. *Mol Plant* **7**: 1494–1496
- Li N, Xu R, Duan P, Li Y** (2018) Control of grain size in rice. *Plant Reprod* **31**: 237–251
- Li R, Xu CG, Yang ZY, Wang XK** (1998) The extent of parental genotypic divergence determines maximal heterosis by increasing fertility in inter-subspecific hybrids of rice (*Oryza sativa* L.). *Mol Breeding* **4**: 205–214
- Li W, Lacey RF, Ye Y, Lu J, Yeh K-C, Xiao Y, Li L, Wen C-K, Binder BM, Zhao Y** (2017) Triplin, a small molecule, reveals copper ion transport in ethylene signaling from ATX1 to RAN1. *PLOS Genet* **13**: e1006703
- Liu L, Fan X-D** (2014) CRISPR–Cas system: a powerful tool for genome engineering. *Plant Mol Biol* **85**: 209–218
- Mandaokar A, Browse J** (2009) MYB108 acts together with MYB24 to regulate jasmonate-mediated stamen maturation in *Arabidopsis*. *Plant Physiol* **149**: 851–862
- Mantouvalou I, Malzer W, Kanngiesser B** (2012) Quantification for 3D micro X-ray fluorescence. *Spectrochimica Acta Part B-Atomic Spectrosc* **77**: 9–18
- Mira H, Martínez-García F, Peñarrubia L** (2001) Evidence for the plant-specific intercellular transport of the *Arabidopsis* copper chaperone CCH. *Plant Journal* **25**: 521–528
- Mitra GN** (2015) Regulation of nutrient uptake by plants. A Biochemical and Molecular Approach. Springer India, New Delhi, India, p. 141–146
- Nour-Eldin HH, Hansen BG, Norholm MH, Jensen JK, Halkier BA** (2006) Advancing uracil-excision based cloning towards an ideal technique for cloning PCR fragments. *Nucleic Acids Res* **34**: e122
- Pautler M, Tanaka W, Hirano H-Y, Jackson D** (2013) Grass meristems I: shoot apical meristem maintenance, axillary meristem determinacy and the floral transition. *Plant Cell Physiol* **54**: 302–312
- Peñarrubia L, Romero P, Carrió-Seguí A, Andrés-Bordería A, Moreno J, Sanz A** (2015) Temporal aspects of copper homeostasis and its crosstalk with hormones. *Front Plant Sci* **6**: 255–255
- Perea-García A, Andrés-Bordería A, Mayo de Andrés S, Sanz A, Davis AM, Davis SJ, Huijser P, Peñarrubia L** (2016) Modulation of copper deficiency responses by diurnal and circadian rhythms in *Arabidopsis thaliana*. *J Exp Botany* **67**: 391–403
- Pilon M** (2017) The copper microRNAs. *New Phytologist* **213**: 1030–1035
- Pilon M, Ravet K, Tapken W** (2011) The biogenesis and physiological function of chloroplast superoxide dismutases. *Biochim Biophys Acta* **1807**: 989–998
- Porebski S, Bailey LG, Baum BR** (1997) Modification of a CTAB DNA extraction protocol for plants containing high polysaccharide and polyphenol components. *Plant Mol Biol Reporter* **15**: 8–15
- Printz B, Lutts S, Hausman J-F, Sergeant K** (2016) Copper trafficking in plants and its implication on cell wall dynamics. *Front Plant Sci* **7**: 601
- Puig S, Mira H, Dorcey E, Sancenón V, Andrés-Colás N, Garcia-Molina A, Burkhead JL, Gogolin KA, Abdel-Ghany SE, Thiele DJ, et al.** (2007) Higher plants possess two different types of ATX1-like copper chaperones. *Biochem Biophys Res Commun* **354**: 385–390
- Radin I, Mansilla N, Rödel G, Steinebrunner I** (2015) The *Arabidopsis* COX11 homolog is essential for cytochrome c oxidase activity. *Front Plant Sci* **6**: 1091–1091
- Rahmati Ishka M, Vatamaniuk OK** (2020) Copper deficiency alters shoot architecture and reduces fertility of both gynoecium and androecium in *Arabidopsis thaliana*. *Plant Direct* **4**: e00288
- Ramamurthy RK, Waters BM** (2017) Mapping and characterization of the *fefe* gene that controls iron uptake in melon (*Cucumis melo* L.). *Front Plant Sci* **8**: 1003
- Ravet K, Pilon M** (2013) Copper and iron homeostasis in plants: the challenges of oxidative stress. *Antioxid Redox Signal* **19**: 919–932
- Regan SM, Moffatt BA** (1990) Cytochemical analysis of pollen development in wild-type *Arabidopsis* and a male-sterile mutant. *Plant Cell* **2**: 877–889
- Sancenón V, Puig S, Mira H, Thiele DJ, Peñarrubia L** (2003) Identification of a copper transporter family in *Arabidopsis thaliana*. *Plant Mol Biol* **51**: 577–587
- Satoh-Nagasawa N, Nagasawa N, Malcomber S, Sakai H, Jackson D** (2006) A trehalose metabolic enzyme controls inflorescence architecture in maize. *Nature* **441**: 227–230
- Schaaf G, Ludewig U, Erenoglu BE, Mori S, Kitahara T, von Wieren N** (2004) ZmYS1 functions as a proton-coupled symporter for phytosiderophore- and nicotianamine-chelated metals. *J Biol Chem* **279**: 9091–9096
- Scholthof K-BG, Irigoyen S, Catalan P, Mandadi KK** (2018) *Brachypodium*: a monocot grass model genus for plant biology. *Plant Cell* **30**: 1673–1694
- Schroeder JI, Delhaize E, Frommer WB, Guerinot ML, Harrison MJ, Herrera-Estrella L, Horie T, Kochian LV, Munns R, Nishizawa NK, et al.** (2013) Using membrane transporters to improve crops for sustainable food production. *Nature* **497**: 60–66

- Schwacke R, Schneider A, van der Graaff E, Fischer K, Catoni E, Desimone M, Frommer WB, Flügge U-I, Kunze R** (2003) ARAMEMNON, a novel database for arabidopsis integral membrane proteins. *Plant Physiol* **131**: 16–26
- Shewry PR, Halford NG** (2002) Cereal seed storage proteins: structures, properties and role in grain utilization. *J Exp Botany* **53**: 947–958
- Shorrocks VM, Alloway BJ** (1988) Copper In Plant, Animal And Human Nutrition. Hertfordshire: Copper Development Association, Potters Bar
- Solberg E, Evans I, Penny D** (1999) Copper deficiency: diagnosis and correction. In *Agri-facts. Soil Fertility/Crop Nutrition*. Alberta Agriculture, Food and Rural Development, Agdex **532–3**, pp. 1–9.
- Tanaka W, Pautler M, Jackson D, Hirano H-Y** (2013) Grass meristems II: inflorescence architecture, flower development and meristem fate. *Plant Cell Physiol* **54**: 313–324
- The International Brachypodium I, Vogel JP, Garvin DF, Mockler TC, Schmutz J, Rokhsar D, Bevan MW, Barry K, Lucas S, Harmon-Smith M, et al.** (2010) Genome sequencing and analysis of the model grass *Brachypodium distachyon*. *Nature* **463**: 763
- Tshikunde NM, Mashilo J, Shimelis H, Odindo A** (2019) Agronomic and physiological traits, and associated quantitative trait loci (qtl) affecting yield response in wheat (*Triticum aestivum* L.): a review. *Front Plant Sci* **10**: 1428–1428
- Tvrda E, Peer R, Sikka SC, Agarwal A** (2015) Iron and copper in male reproduction: a double-edged sword. *J Assisted Reprod Genetics* **32**: 3–16
- Vogel J, Hill T** (2008) High-efficiency agrobacterium-mediated transformation of *Brachypodium distachyon* inbred line Bd21-3. *Plant Cell Reports* **27**: 471–478
- Vollbrecht E, Springer PS, Goh L, Buckler IV ES, Martienssen R** (2005) Architecture of floral branch systems in maize and related grasses. *Nature* **436**: 1119–1126
- Waters B, Chu H, Didonato R, Roberts L, Eislely R, Lahner B, Salt D, Walker E** (2006) Mutations in Arabidopsis yellow stripe-like 1 and yellow stripe-like 3 reveal their roles in metal ion homeostasis and loading of metal ions in seeds. *Plant Physiol* **141**: 1446–1458
- Weber E, Gruetzner R, Werner S, Engler C, Marillonnet S** (2011) Assembly of designer TAL effectors by golden gate cloning. *PLOS ONE* **6**: e19722
- White PJ** (2012) Chapter 3—long-distance transport in the xylem and phloem A2—Marschner, Petra. In *Marschner's Mineral Nutrition of Higher Plants (Third Edition)*. Academic Press, San Diego, pp 49–70
- White PJ, Broadley MR** (2009) Biofortification of crops with seven mineral elements often lacking in human diets—iron, zinc, copper, calcium, magnesium, selenium and iodine. *New Phytologist* **182**: 49–84
- Wieser H, Antes S, Seilmeier W** (1998) Quantitative determination of gluten protein types in wheat flour by reversed-phase high-performance liquid chromatography. *Cereal Chem* **75**: 644–650
- Yamaji N, Ma JF** (2014) The node, a hub for mineral nutrient distribution in graminaceous plants. *Trends Plant Sci* **19**: 556–563
- Yamasaki H, Hayashi M, Fukazawa M, Kobayashi Y, Shikanai T** (2009) SQUAMOSA promoter binding protein-like7 is a central regulator for copper homeostasis in *Arabidopsis*. *Plant Cell* **21**: 347–361
- Yan J, Chia J-C, Sheng H, Jung H-i, Zavodna T-O, Zhang L, Huang R, Jiao C, Craft EJ, Fei Z, et al.** (2017) Arabidopsis pollen fertility requires the transcription factors C1TF1 and SPL7 that regulate copper delivery to anthers and jasmonic acid synthesis. *Plant Cell* **29**: 3012–3029
- Yordem BK, Conte SS, Ma JF, Yokosho K, Vasques KA, Gopalsamy SN, Walker EL** (2011) *Brachypodium distachyon* as a new model system for understanding iron homeostasis in grasses: phylogenetic and expression analysis of Yellow Stripe-Like (YSL) transporters. *Ann Botany* **108**: 821–833
- Yuan M, Li X, Xiao J, Wang S** (2011) Molecular and functional analyses of COPT/Ctr-type copper transporter-like gene family in rice. *BMC Plant Biol* **11**: 69
- Zhai Z, Gayomba SR, Jung H-i, Vimalakumari NK, Piñeros M, Craft E, Rutzke MA, Danku J, Lahner B, Punshon T, et al.** (2014) OPT3 is a phloem-specific iron transporter that is essential for systemic iron signaling and redistribution of iron and cadmium in *Arabidopsis*. *Plant Cell* **26**: 2249–2264
- Zhai Z, Sooksa-nguan T, Vatamaniuk OK** (2009) Establishing RNA interference as a reverse-genetic approach for gene functional analysis in protoplasts. *Plant Physiol* **149**: 642–652
- Zhang B, Ye W, Ren D, Tian P, Peng Y, Gao Y, Ruan B, Wang L, Zhang G, Guo L, et al.** (2015) Genetic analysis of flag leaf size and candidate genes determination of a major QTL for flag leaf width in rice. *Rice* **8**: 2
- Zhang C, Lu W, Yang Y, Shen Z, Ma JF, Zheng L** (2018) OsYSL16 is required for preferential Cu distribution to floral organs in rice. *Plant Cell Physiol* **59**: 2039–2051
- Zheng L, Yamaji N, Yokosho K, Ma JF** (2012) YSL16 is a phloem-localized transporter of the copper-nicotianamine complex that is responsible for copper distribution in rice. *Plant Cell* **24**: 3767–3782